PCCP

Accepted Manuscript

ROYAL SOCIETY OF CHEMISTRY

www.rsc.org/pccp

Cite this: DOI: 10.1039/c0xx00000x

www.rsc.org/xxxxxx

ARTICLE TYPE

Fluorescence from graphene oxide and the influence of ionic, π-π interactions and heterointerfaces-electron or energy transfer dynamics

Sesha Vempati,*[a] and Tamer Uyar*[ab]

Received (in XXX, XXX) Xth XXXXXXXXX 20XX, Accepted Xth XXXXXXXXX 20XX

DOI: 10.1039/b000000x

2D crystals such as graphene and its oxide counterpart sought good research attention for their application as well as fundamental interest. Especially graphene oxide (GO) is quite interesting because of its versatility and diverse application potential. However the mechanism of fluorescence from GO is under severe discussion. To explain the emission in general two interpretations were suggested, *viz* localization of sp^2 clusters and involvement of oxygeneous functional groups. Despite of this disagreement, it should be acknowledged that the heterogeneous atomic structure, synthesis dependent and uncontrollable implantation of oxygenfunctional groups on the basal plane makes such explanation more difficult. Nevertheless, a suitable explanation enhances the applicability of the material which also enables the designing novel materials. At this juncture we believe that by given the complexity in understanding the emission mechanism it would be very useful to review the literature. In this perspective we juxtapose various results related to fluorescence and influencing factors so that a conclusive interpretation may be unveiled. Apparently, the existing interpretations have largely ignored the factors such as self-rolling, byproduct formation etc. *Vis-a-vis* previous reviews did not discuss the interfacial charge transfer across heterostructures and the implication on the optical properties of GO or reduced graphene oxide (rGO). Such analysis would be very insightful to determine the energetic location of sub band gap states. Moreover, ionic and π-π type interactions are also considered for their influence of emission properties. Apart from these, quantum dots, covalent modifications and nonlinear optical properties of GO and rGO were discussed for completeness. Finally we made concluding remarks with outlook.

Introduction

Graphene (Gra) in its pure form has attracted a lot of research attention.[1,2] Notably its oxidized form, graphene oxide (GO) has also sought equal importance [2-6] because of the application potential in electronic devices,[7-9] biomedical and environmental remedies. Initially, in 1860 Brodie [10] produced graphite oxide (presently known as graphene oxide) for the first time and later Staudenmeier [11] in 1898 and Hummers et al.[12] in 1958 have synthesized the same. Other applications include transparent conductive coatings in pure form [7,13] to improve the hole transporting property,[9] flexible optoelectronics [14] and white light fluorophores [15] when combined with potential material such as ZnO.[16-22] A control on the reduction level enables the band gap tunability [23] while its solution processibility to make large area thin films is worth mentioning.[24] The band gap tunability permits its application in mid-IR range photodetectors. Furthermore GO is integrated with silicon [8] which suggests its suitability in industry. On the other hand biomedical applications include cell imaging,[25] drug delivery,[25,26] photothermal therapy and photoacoustic imaging,[27] detection of Cu^{2+} ions,[28] alcohol sensor,[29] biosensor,[3,30] *in vivo* toxicology effects [31] etc. See a review article by Morales-Narvaez et al. for optical bio sensing applications of GO.[30] Environmental remedies include photocatalysts [29,32,33] when combined with semiconductors such as ZnO, ZnS,[29] titanosilicate [33] etc. It is notable that the presence of another semiconductor is vital; hence the role of GO or reduced graphene oxide (rGO) is to delay the recombination process in the semiconductor.[32] Figure 1 (top) shows number of publications against year. We can see the intensity of research in recent past on GO and related materials. In Figure 1 (bottom) we have created a tabular form in which the distribution of research areas against the number of publications is given. These data are convincing that the research interest on GO is constantly growing by given its applicability in a range of research areas.

Fluorescence from graphene should be phonon assisted [34] because of its zero band gap. In clear contrast, GO and rGO has shown NIR, visible and UV fluorescence [15,25,26,35-39] with a quantum efficiency of 6.9%.[40] Luminescence of GO is also reported in red and NIR regions [26,38] which can result from the presence of multilayered and aggregated flakes.[36] Importantly, the mechanism which describes the fluorescence of GO or rGO is under severe discussion suggesting two different interpretations. One of them is the localization of sp^2 clusters where the quantum confinement effect splits the energy bands and the recombination of *e/h* pairs gives luminescence. The second explanation involves O2*p* orbital where the CB of the localized GO sp^2 domains can be

assigned to the π* orbitals, while the VB changes from the π to the O2*p* orbitals. In the former case, oxygen-related functional groups are eliminated from the emission mechanism due to the enhancement of fluorescence upon reduction.[15,36,39] O2*p* orbitals are eliminated despite of the fact that the method of reduction plays a crucial role in case if the process enhances radiative or non-radiative paths.[41] Interestingly, as mentioned earlier, the band gap of GO is controllable [23] via manipulating the reduction level. However, rGO is associated with a set of defects such as remnant oxygen atoms,[42] pentagon–heptagon pairs (Stone–Wales defects) [43,44] and holes [44,45] due to the loss of carbon from the basal plane.[46] Especially with the chemical reduction, hydrazine is found to be efficient to remove in plane functional

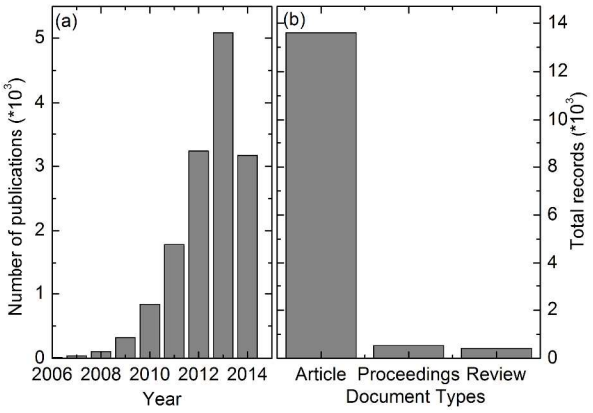

Research Areas	Records
Chemistry	8854
Materials science	7176
Science technology other topics	3963
Physics	3864
Electrochemistry	1528
Engineering	1058
Energy fuels	968
Polymer science	646
Biophysics	295
Biotechnology applied microbiology	248
Environmental sciences ecology	215
Instruments instrumentation	215
Optics	207
Biochemistry molecular biology	151
Metallurgy metallurgical engineering	113

Fig. 1 (top) (a) Number of publications against year and (b) shows the number of articles reviews and proceedings those have appeared until now. Table (bottom) shows the distribution of research areas against number of publications. Data analyzed from web of knowledge as of 7th July 2014, key word for (a) graphene oxide

groups (epoxy and hydroxyl), however, the edge moieties (carboxyl and carbonyl) stay undisturbed.[47-49] In addition, it is also found that hydrazine reduction creates new functional groups such as C=N on the rGO.[50-53] To emphasize, it is vital to elucidate a suitable mechanism for the luminescence of GO and rGO. This should be able to explain the influence of various factors such as reduction level against luminescence properties. Appropriate mechanism allows us to design new material combinations where GO and rGO can be further exploited.

In the present perspective we have avoided the GO-synthesis details, however, please refer to an earlier article in which various chemical methods are discussed in the view point of large-area thin-film electronics and optoelectronics.[5] Structural, electronic, optical and vibrational properties of nanoscale carbons and nanowires are discussed in a review by Cole et al.[4] Graphene-based nanomaterials in optical and optoelectronic applications were reviewed by Chang et al.[54] Given the background and disagreements in interpreting the emission mechanism necessitates its understanding of the current state of art. Hence in this perspective we critically discuss various results from the literature in an attempt to provide a clear insight to those explanations. We also cover the role of prominent functional groups and tunable band gap, excitation dependent emission process, quantum dots (QDs), doping-effect on the emission properties, nonlinear optical properties and influence of noncovalent/covalent functionalization. By given the contextual nature, we have briefly discussed various reduction processes and their effects as well. We will see that during the reduction process removal of oxygen is as inevitable as the formation of other complex bonds. Furthermore we have discussed ionic interactions such as pH dependency and interaction with other ionic species including the π-π type. Finally, heterointerfaces and the consequent charge transfer mechanism are discussed in relation to photovoltaics and nanocomposites.

2. Reduction of graphene oxide

In the context of applications a scalable method is demanding to produce potential materials such as GO or rGO. The excellent properties depicted by these materials require mass production within the lines of well established and industrially applicable procedures. GO in its oxidized form is less conducting (of course depending on the level of oxidation) because of the distorted conjugation. It is important that we meet the above mentioned criteria. In this context one of the ways forward is the reduction of exfoliated GO. We can retrieve the electrical properties of GO to an extent by chemical and thermal reductions.[35] To date, the rGO sheets reduced by hydriodic acid and acetic acid have shown the best electronic conductivity (up to 30 000 S/m).[55] The 'retrieval of conductivity' is not the main objective of this section. Nevertheless the methods discussed here are in fact correlated with the emission properties. For example, in a molecular dynamics simulation the formation of highly stable carbonyl and ether groups is inevitable in a thermal reduction process.[56] Hence the optical properties depicted by thermally reduced GO should consider the presence/formation of these functional groups and associated influence on the emission properties. In the following we have mentioned some of the techniques such as thermal,[35,57] photo-thermal [58] and chemical [6,35,59] reductions. Various other reducing agents and techniques can be seen from Ref.[5] For the following reagents, see the cross references in the given citation. Ammonia, $NaBH_4$, supercritical water, sugar and ascorbic acid [60]; bovine serum albumin, bacterial respiration and hydriodic acid [61]; hydroquinone, strong alkaline media, sulfur-containing

compounds and amines [62]; electrochemical and photographic camera flash.[63] Reduction in principle decreases the density of oxygeneous functional groups, while the selectivity is of course process dependent. The presence of residual oxygen-containing functional groups and defects are detrimental for various applications. These active sites make the surface reactive and provide the tunability in electronic and optoelectronic properties via chemical reactions,[36,43,64] including their incorporation in nanocomposites.[65]

When compared to hydrazine, hydriodic acid is less toxic and may be employed for the mass production of rGO dispersions. Controlled ozone treatment can tune the electrical and optical properties of graphene [66] via oxidation. Thermal reduction is another versatile and industrially applicable process to reduce GO.[35] Low temperature thermal reduction is implemented on large area self assembled GO films.[57] Furthermore, in photothermal reduction UV light impinges on the samples which are simultaneously subjected to heating. This is quite interesting method where a precise control on the reduction level can be obtained,[58] especially in the lab scale environment for synthesizing novel derivatives of GO.

In the context of chemical reduction, hydrazine and its derivatives are rather potential as reducing agents which were extensively studied in the literature.[35] The important consequences of employing hydrazine in vapor or liquid phase are discussed in section 3.2. To draw readers' attention to one of the key features, a study by Mathkar et al.[59] shows the band gap tunability by simply varying the exposure time of hydrazine vapor (will be discussed, Figure 5). Oxygen plasma treatment is a better method in some aspects when compared to that of hydrazine. The oxygen plasma treatment creates much cleaner rGO [67] while converting the epoxy groups into carbonyl groups though limited to the surface for a multilayered sample. Interestingly, oxygen plasma treatment can convert non-emitting graphene into broad red-NIR emitting layer [68] with spatial uniformity. While hydrazine treatment is prone to create C=N bonds.[50,53]

Emission properties of GO

3.1 Fluorescence of luminescence?

Several authors refer the emission from GO as photoluminescence (PL). However, by given the time scales of the decay process it would be appropriate to refer the emission as fluorescence (PL occurs in the order of ps). For example, lifetimes are below 6 ns for multicolour fluorescent GO which is synthesized by cleaving CNT upon oxidation.[69] Some examples of decay times for various combinations of GO or rGO with other materials were tabulated in Table 1. Also the details of excitation and emission wavelengths were given where available. From the table, it is clear that the decay times are in the order of nanoseconds. Nevertheless it is notable that the total decay curve might an integral of more than one decay process.[70] It is important to note that the number of components is determined by the chemistry of the material and the relative stability of the intermediate states. A better understanding of the emission properties can perhaps suggests an appropriate number of decay constants.

3.2 Mechanism of fluorescence

If fluorescence has to occur in Gr then it must be assisted by phonons [34] because of its zero band gap. In clear contrast to GO and rGO with heterogeneous atomic and electronic structures depicted UV, visible and NIR fluorescence.[6,15,25,26,35-39] On the other hand, UV-Vis emission from carbon based materials (amorphous,[71-73] disordered carbons [74-76]) is known. However, band gap tunability and solution processability of GO enables its versatility in various applications.[6] Previously (Section 3.1, Table 1) we have broadly seen the emission wavelengths and their decay times of GO and rGO in pure form or when attached to other functional material via covalent or noncovalent means. Note that as-synthesized GO did not emit light at all instances.[37,77] On the other hand emission at specific wavelengths, for example, 440 nm,[15] 505 nm [31] and blue-UV region [15,36,39] were observed. The emission wavelengths of GO depend on the functional groups,[45] pH [69,78-82] and its combination with other materials such as PANI-nanorods,[83] MB,[84] tetra-amino porphyrin,[85] PEG [25,26] etc. Since the emission from GO is dependent on various factors, one should go deeper to understand the mechanism. Strong heterogeneity in atomic and electronic structure makes the emission process quite complex. Fluorescence from GO arises from the recombination of *e/h* pairs in localized electronic states of various configurations. Having said that, the exact mechanism is still unknown. However, researchers have attempted to provide some crucial insights and interpretation for their observations, which we summarize below. Before we go into those details, excitation dependent fluorescence will be discussed.

GO depicts excitation dependent emission as observed by many groups.[86-88] The reason for excitation dependency is that different transitions are possible from the CBM and nearby localized states to the wide-range VB. While the lack of emission for the excitation above the band gap [5,37] can be due to the fact that the excitation energy is either dissipated as heat or injected into the adjacent metallic phase of carbon sheet.[77]

The emission from GO is in clear contrast to the general semiconductors. In the case of general semiconductors the band edge transition and subsequent recombination yields PL. One of the explanations given for the fluorescence of GO is as follows. The fluorescence from GO arises from *e/h* recombination in localized sp^2 electronic states which are confined within the sp^3 matrix, i.e. confinement of π-electrons (please see section 3.4 for size dependent effects).[71-73] Although sp^2 clusters are under quantum confinement,[6] there are no discrete energy levels, however the local energy gap is determined by the cluster size. It means that for a given sample, the size differences in the clusters produce multiple wavelengths. Hence the attribution of wavelengths to the 'average cluster size' needs to be handled carefully especially when wavelength specific applications are considered. It is notable that GO gives fluorescence when the concentration of sp^2 cluster is optimum,[36] passivated reactive sites,[89] chemical bonding with fluorescent ions,[90] or in the form of QDs.[37] Typical electronic structure of GO can be schematized as shown in Figure 2, where the black arrows denote the transitions of electrons and

Table 1 Decay times for various combinations of GO or rGO and mechanism if attributed.

S.NO	Compound	Excitation λ_{ex} (nm)	Emission λ_{em} (nm)	Decay time (ns)			Mechanism/comment	Ref
				τ_1	τ_2	τ_3		
1	GO from cleaved CNT	365	38-690	5.1			localized sp^2 clusters.	69
2	rGO	318	all	5	1.2	0.2	π-π type noncovalent attachment	70
	Rb	375	400-700	4.76				
	rGO–Rb noncovalent	358	440					
		362	460					
3	GO QDs	NA	NA	~5.4				28
	GO QDs/Cu^{2+}	NA	NA	~5.4			complexation (static quenching)	
4	P^+	438[a]	640	~20				91
	GO/P^+	438[a]	640	1.2	6		e^- and/or energy transfer from P^+ to GO, donor acceptor complex	
	P^-	438[a]	640	$12<\tau_1<20$[b]				
	GO/P^-	438[a]	640				no interaction: repulsion between similar charges	
5	P3HT	400[c]	575	0.748			covalent bonding: π–π interaction dynamic quenching and forming a non-fluorescent GOund-state complex	92
	GO/P3HT	400[c]	575	0.532				
	rGO/P3HT	400[c]	575	0.351			charge pairs are injected into GO as fast as 1.4 ps	

[a] 250 ps pulse width; [b] approximated from graph as the actual value was not given; [c] ~46 nJ/cm^2;

holes under suitable illumination (E_{exc}). Upon absorbing E_{exc}, *e/h* pairs are created followed by non-radiative relaxation and radiative recombination emitting E_{PL}. The emission bands are dependent on electronic band gaps of sp^2 clusters (mixture of sp^2 and sp^2 bonding).[71,93,94] Moreover the band gap is associated with the size, shape, and fraction of the sp^2 clusters located within the sp^3 matrix.[36] For instance smaller sp^2 clusters depicts wider energy gaps because of the relatively higher quantum confinement effect. By given a range of sp^2 cluster size, it is hard to distinguish the features depicted by each cluster. Hence an integral effect is generally seen. Most of the synthesis methods are not very successful in producing GO with a controlled or predetermined cluster size. Further details on how to calculate the cluster size were given in Section 3.4.

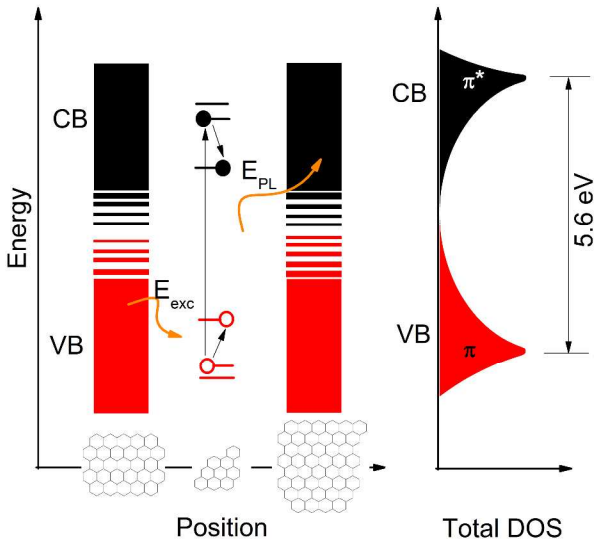

Fig. 2 (Color online) Schematic band structure of GO. Smaller sp^2 domains have a larger energy gap due to a stronger confinement effect. DOS-electronic density of states. Figure redrawn after Ref.[36]

There is an alternative explanation given in the literature for fluorescence from GO.[37] In this investigation the authors have used hydrothermal technique to cut GO sheets into QDs which emit blue color. The authors suggested that the emission occurs from zigzag sites, where their ground state is in triplet state similar to carbene. This can be described as $\sigma^1\pi^1$ as shown in Figure 3. The argument is based on the fact that the fluorescence originates from the oxygeneous functional groups as seen earlier in the case of carbon nanoparticles,[75,76,95] functionalized CNTs [74,96] and surface-oxidized Si nanocrystals.[97] However, Loh et al.[6] suggest that the enhancement of fluorescence with reduction excludes oxygen containing functional groups from the possible origin.[15,36,39] Although it is convincing the exclusion is drawn based on the references [15,36] and [39]. According to Loh et al.[6] the localized sp^2 cluster and structural defects during the reduction [98] seemed to be more suitable explanation for the origin and the enhancement of blue fluorescence.[36] On the other hand Chien et al. suggested that the visible emission might arise from defect related states within an interface.[58]

By given the following reasons it is vital to discuss and reconsider the previous argument (sp^2 cluster localization) given to explain the emission from GO. Upon reduction, it is true that the density of oxygen containing functional group decreases. The fluorescence intensity or QY, of course, depends on various factors such as absorption efficiency and the balance between radiative and non- radiative recombinations. Oxygen containing functional groups are eliminated from the emission mechanism due to the enhancement

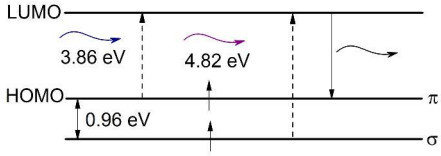

Fig. 3 Schematic of electronic structure at zigzag edge site similar to carbene. Dashed (excitation) and solid arrows (relaxation) for σ- and π-states. Figure redrawn after Ref. [37]

of fluorescence upon reduction.[15,36,39] Conjointly, the method of reduction is a key factor to consider, in case if the process enhances radiative or non-radiative paths. For example, in Ref.[15] three different methods were employed to reduce the GO yielding Gra. *Viz* thermal exfoliation at high temperatures, heating nanodiamond in an inert atmosphere and arc discharge of graphite electrodes in the presence of H_2/He. This few-layer-Gra was subjected to acid treatment under microwave irradiation to yield GO. Subrahmanyam et.al.[15] suggest blue emission centred around 400 nm from as prepared Gra-samples, which implies that complete conversion of GO into Gra did not take place through the above three reduction processes. To emphasize, fluorescence in Gra is assisted by phonons.[34] Apart from the above mentioned differences, the intensity scale on the fluorescence spectra or the details of QY were not given by the authors in Ref.[15] In Ref.[36] the authors have used hydrazine for the reduction of GO. It is undisputed that hydrazine treatment decreases the density of oxygen containing functional groups. However some of the reports suggest enhancement of blue fluorescence and quenching of the initial yellow-red fluorescence [39] in addition to the following points. In the case of exposure to hydrazine vapor the functional groups are reduced in the following order as suggested by Mathkar et al.[59] (i) phenol and carbonyl groups are the first to be reduced then (ii) epoxide moieties and finally (iii) tertiary alcohols. In this context it is notable that the electron withdrawing capacity (acidity) depends on the functional group, thereby a variation in the electron DOS of rGO is expected. Furthermore, hydrazine treatment can form C=N [50,99-101] bonds on rGO. It is also found that the fluorescence intensity of GO is greatly enhanced with no spectral shift after a short exposure of hydrazine vapors.[36] During hydrazine monohydrate reduction XPS has evidenced C=N functional groups,[99] resulting from a reaction as explained in the Refs.[100,101] Furthermore, the reduction of GO is accompanied by some nitrogen incorporation from the reducing agent (C/N = 16.1 by elemental analysis). This is presumably through a reaction of hydrazine hydrate with the carbonyl groups of GO.[51] Notably, the incorporation of 'N' in the rGO is suggested to take place via other functional groups such as lactones, anhydrides, quinones with which hydrazine can react.[51] Hydrazine is found to be efficient to remove in plane functional groups such as epoxy and hydroxyls, however, the edge moieties such as carboxyl and carbonyl stay intact.[47-49] Another study suggests that the hydroxyls on the basal planes of GO were not removed by hydrazine hydrate even at elevated temperature.[50] Furthermore this study also suggests that the carbonyl and carboxylate groups formed the C=N bonds of hydrazones.[50] After hydrazine vapour treatment,[53] incorporation of nitrogen at substantial level was confirmed by XPS analysis and attributed to partial reduction of carbonyl groups to hydrazone groups.[51,52] It is also important to consider the synthesis method of GO against the hydrazine reduction process as the former play a major role in determining the functional groups, density and their physical location on graphitic plane. As the reduction takes place the distance between the sheets decreases because of the π-π interactions. By given the discrepancy in the literature, it is highly recommended that the effect of hydrazine on the type (synthesis method) of GO requires thorough investigation. .

In the context of GO QDs, the fluorescence intensity from as synthesized QDs is higher than its annealed (200°C in vacuum) counterpart apart from a blue shift.[36] During thermal annealing process, formation of intermediate phases were observed by Jeong et al.[102] These phases were attributed to the conversion of hydroxyl groups into epoxide and carboxyl groups. As a consequence the interlayer distance is increased and the carbon backbone switches to a sp^3 structure.[102] Similar observation and attribution is suggested in a study by Cuong et al.[103] Furthermore in molecular dynamics simulations the formation of highly stable carbonyl and ether groups was observed in the thermal reduction process.[56] Hence the optical properties depicted by the thermally reduced GO should consider the presence of these functional groups and associated influence on the emission properties.

The existence of O2*p* level and its active participation were discussed in the context of TiO_2/GO heterointerface (Figure 18d).[77] In this study IOT (reduced symmetry at the interface,[104] type-II fluorescence [105]) was observed between TiO_2 and the O2*p* of GO. Under suitable illumination, the electrons localize in the CB of TiO_2 while the holes can either relax to a defect level or injected to the O2*p* level. The optical recombination of electrons from CB of TiO_2 with that of holes in O2*p* levels of GO gives fluorescence (IOT). The details of IOTwill be discussed more elaborately in Section 7.2.

To point out another important study by Zhang et al.[106] in which the authors have studied the optical properties against self-rolling effect of chemically derived graphene sheets. For concentrations less than 10 mg/mL, these sheets have shown self-rolling, and aggregated for higher than the said value. The earlier studies in which the fluorescence quenching effect is reported may be reconsidered, as the rolling of sheets severely influences the electronic absorption and emission properties. As a matter of fact, numerous studies evidenced that Gra acts as an electron reservoir, where the photogenerated electrons are collected from an adjacent/accompanying semiconductor.[29,32,33] Aggregated sheets have shown a clear deviation from Beer-Lambert law. Apart from these, the absorptivity was decreased and spectral shapes were changed. Rolled sheets depicted new absorption (at 500 and 960 nm) and emission (after 500 nm) bands with decreased emission efficiency.[106] Furthermore this study also suggests that the emission mechanism for single and double layered GO or rGO needs to be re-examined. Self-rolling can be avoided by choosing an appropriate solvent, however, it associates another complexity such as 'dielectric constant' as it plays a key role in the emission process and its energy.[6] Having said that, for sheet dimensions in the range of 1-10 μm, their dispersion and solid sample have shown comparable fluorescence.[38] Extending the argument of self-rolling, with increasing reduction level the π-π interaction among the sheets also increases and hence the carrier dynamics may be influenced significantly. Finally, similar to the effects from 'hydrazine reduction', the effect of 'dielectric constant' should be investigated further.

In the band diagram of second explanation for the fluorescence, the CB of the localized sp^2 domains are assigned to the π* orbitals, while the VB changes from the π to O2*p* orbitals.[41] Ref.[41] contains discussion of the results from local DFT simulations via first-principles. The energy of the indirect band gap increases with the increasing degree of oxidation, e.g.

~2.7-3.2 eV for the GO samples studied in Ref.[107] Relatively higher band gap causes extremely weak absorption for GO in the visible range.[90,107] The changing of VB from the π to the O2*p* orbitals is also suggested by Jeong et al. where the HOMO level shifts downwards opening the band gap.[108] It will be very useful, if wavelength selective photodetectors based on GO or rGO are studied while combining the well understood materials. This allows us to elucidate the energetic location of bands and carrier dynamics there in.[18]

3.3 Role of prominent functional groups, tunable band gap

In the previous section we mainly discussed two mechanisms that may describe the fluorescence in GO and rGO. In this section we will see how the functional groups inflect the optical properties.[45] It is vital because when GO is reduced with hydrazine (section 3.2) the oxygen related functional groups follow a sequence [59] where phenol and carbonyl groups are the first and tertiary alcohols are the last to be reduced. An experimental investigation on GO and rGO has also suggested that the oxygeneous functional groups play a major role in determining the band gap.[23] A mixture of oxygen and hydroxyl groups with coverage of 100 %, 75 %, 50 % depicted band gaps of ~2.8, 2.1 and 1.8 eV, respectively.[23] The control on the density and coverage of these functional groups allows us to tune the band gap of rGO. In a study by Johari et al.[45] *ab initio* DFT based simulations were performed to understand the electronic and optical properties of periodic structures. In this investigation [45] GO with different coverage densities and compositions of functional groups (epoxides, hydroxyls and carbonyls) were studied. The key findings were as follows. (i) Optical band gap decreases rapidly (4.0 to 0.3 eV) with an increase in the size of the hole or defect in the case of carbonyl groups (O to C ratio from 0 to 37.5 %). When epoxy and hydroxyl functional groups vary from 25 to 75%, π+σ plasmon is found to depict a significant blue shift (~1.0-3.0 eV) unlike the π plasmon peak which is less sensitive. Furthermore, the increase in carbonyl groups on the basal plane creates holes and consequently the π plasmon peak is shifted by ~1.0 eV when compared to that of the pristine Gra. This study supports the earlier argument of method of synthesis is an important factor to consider, where the density of these oxygeneous functional groups vary depending on the process. Taking the discussion a step forward, if the epoxy groups on GO are converted (oxygen plasma treatment) into carbonyl groups [67] apart from the excitation dependency, the luminescence spectra depicted distinct features (Figure 4). As the oxygen pressure increases (GO-2 to GO-4:sp^3 hybridization increases) the shoulder at 530 nm disappears apart from a spectrally invariant emission at 487 nm. Clusters of larger size are more prone to oxidation introducing nonradiative paths (epoxy & carbonyl) and dangling bonds which result in quenching of emission at longer wavelength (550–650 nm). Interestingly, the QY increases from GO-2 to GO-4 compared to GO-1.[109] The emission has occurred from a range of GO dimensions, where red to NIR is observed in nanosized aqueous GO dispersions.[25,26] Note that the GO in these two cases is functionalized with PEG.

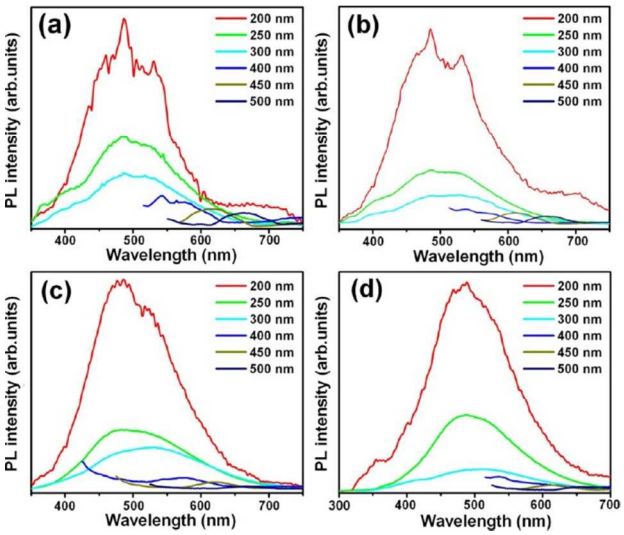

Fig. 4 (Color online) Fluorescence spectra for (a) GO-1, (b) GO-2, (c) GO-3, and (d) GO-4 films at different λ_{ex}. Reproduced with permission from Ref. [67]

Experimentally a control on the reduction of functional groups of GO is achieved through hydrazine vapor exposure. It enables the band gap tunability from 3.5 to 1 eV (Figure 5).[59] Refer to section 3.2 for more details related to this method of reduction. Within the first 8 h of hydrazine exposure the optical band gap is seen to fall rapidly from a starting point of 3.5 eV. Precise control on the reduction time yields the band gap that we require, however, the density of functional groups cannot be controlled with this process. As an aside, spectroscopic ellipsometry can be employed to estimate the band gap by applying Lorentz oscillator model which provides accurate energy level distribution in GO or rGO.[23,110] Apart from UV-Vis spectroscopy, cyclic voltametry can be used with which the edges of CB and VB can be determined.[59] Crucially, it should be unveiled whether these techniques yield comparable results for GO and rGO in the background of their complex band structure. Controllable oxidation of Gra is also a subject of investigation [111] however, Wang et al. did not provide an estimation of band gap for different oxidation levels.

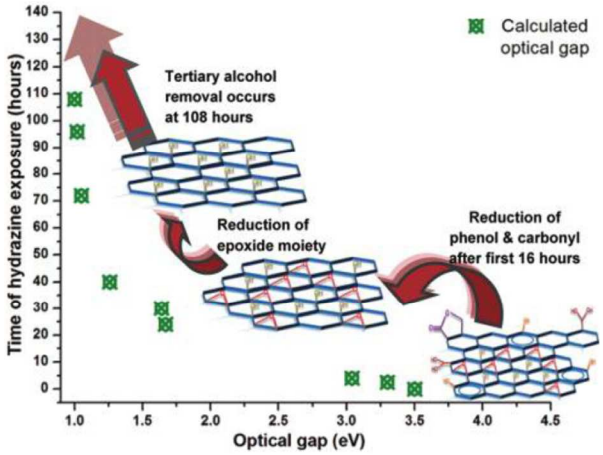

Fig. 5 Band gap modulation upon exposure to hydrazine vapors along with a schematic rGO structure at selected time intervals. Reproduced with permission from Ref. [59]

3.4 Quantum dots

The applications of GO QDs have spread into biomedical engineering because of their size dependent emission properties. They are cell imaging, drug delivery,[25] selective detection of Cu^{2+} ions [28] etc. Notably the size dependent emission of GO QDs is similar to that of carbon QDs.[75] GO QDs were synthesized variously.[37,112] For example 1–4 nm (referred as graphene quantum dots in Ref.[112]) sized QDs were synthesized form carbon fibers which not only offer cheap alternative route but also a control on the size enables tunable fluorescence.[112] *In vivo* toxicology effects are also studied for carboxylated GO QDs [31] (Figure 6). In Figure 6 schematic of synthesis, TEM, DLS and fluorescence properties (at 505 nm) were shown for carboxylated GO QDs. KB cells were treated with these carboxylated GO QDs and the corresponding CLSM images is shown. Density gradient ultracentrifuge is employed to obtain monodisperse GO QDs [113] where the UV-Vis and fluorescence spectra revealed that the properties of samples are highly dependent on their sheet size and degree of oxidation. Eda et al.[36] attributed the emission to quantum confinement of sp^2 clusters which in turn connects to its band gap.[71,93,94] Moreover the band gap depends on the size, shape and fraction of the sp^2 clusters.[36] Initially the cluster size (L_a, Å) was estimated by Tuinstra et al.[114] in 1970 by an empirical relation as $L_a = 43.5\ (I_D/I_G)^{-1}$ which was later verified by Knight et al.[115] with additional data points. Note that the method shown in Ref.[114] underestimates the crystallite size if there is a dominant effect of small crystallites, despite it validates the crystallinity from XRD. However, the linear relation suggests that the Raman intensity is proportional to the 'boundary' in the sample.[114] UV-Vis

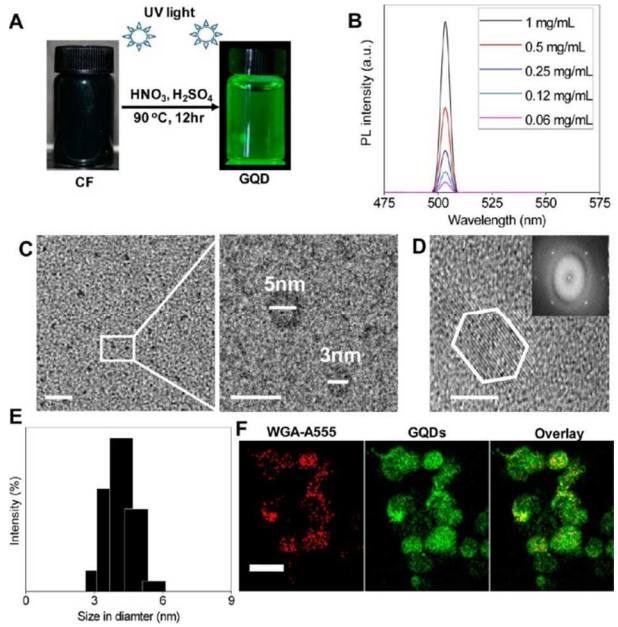

Fig. 6 (A) Synthesis and fluorescence of GO QDs, (B) fluorescence intensities at 505 nm wavelength, (C) TEM images; scale bar is 50 nm for left image and 10 nm for the right image, (D) HR-TEM image (scale bar = 5 nm) showing the edge structure of lattices formed in QDs, inset shows Fourier transformed image, (E) size distribution of the carboxylated Gr QDs measured by DLS and (F) CLSM images of KB cells treated with the carboxylated QDs (scale bar = 50 μm). Reproduced with permission from Ref. [31]

(sp^2 clusters size < 1 nm) and red-IR emission (sp^2 cluster size > 2 nm) is observed by Eda et al.[36] As synthesized GO has larger sp^2 cluster size (4.83 nm) with narrower band gap emitting green-to-red region. After annealing, the cluster size (3.95 nm) as well as emission intensity is decreased apart from a blue shift in the emission spectrum. Other studies have shown similar results for sp^2 cluster sizes of 2.5–8 nm.[5,38,43,71,94,103,116-121] The authors attributed the decreased cluster size to the nucleation of sp^2 domains in the sp^3 matrix. For the cases in which thermal process is employed for the reduction the earlier discussed consequences should be considered (Section 3.2).

GO QDs (referred as graphene quantum dots) were synthesized by Peng et al. [112] where the variance in the size offers tunable band gap and consequently the emission characteristics can be controlled. The UV-Vis absorption spectra were shown in Figure 7 of GO QDs synthesized at 80, 100, and 120 °C. See the inset of Figure 7 for digital photographs under UV light. A clear blue shift is noticed from 330 to 270 nm with increasing synthesis temperature. The fluorescence spectra (Figure 7b) can be understood from the average sizes, shape and defect densities.[64] The size differences may cause variation in density and nature of sp^2 sites, which results in varying band gap (3.90 to 2.89 eV).

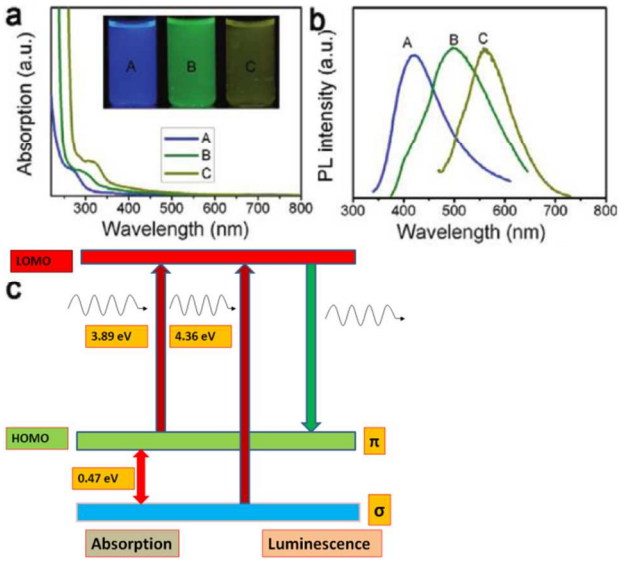

Fig. 7 (a) UV–Vis spectra of GO QDs A, B, and C, corresponds to the reaction temperatures at 120, 100, and 80 °C, respectively. Inset of panel a is a photogaph GO QDs under 365 nm illumination. (b) fluorescence spectra for λ_{ex} 318 (A), 331 (B), and 429 nm (C) and (c) electronic transitions of triple carbenes at zigzag sites observed in the optical spectra for blue emission. Reproduced with permission from Ref. [112] while part c is taken from its supplementary information.

Note that this trend is similar to quantum confinement effect at lower particle sizes (1–10 nm).[122] From the PLE spectra two new transitions (at 284 and 318 nm) were seen, where they can be considered as a transition from the σ and π orbital (HOMO) to the LUMO (Figure 7c) in contrast to π–π* transition. In the case of carbine for a triplet ground state energy differences between the σ and π orbital should be below 1.5 eV,[123,124] where it is 0.47, 0.82, and 1.24 eV for blue, green and yellow emission, respectively.

Under alkaline conditions, the GO QDs emit strong fluorescence, while acidic conditions quench the PL, because the free zigzag sites are protonated while forming a complex.[112] In general the quantum sized materials, of course behave differently from their bulk counterparts. Nevertheless, sp^2 clusters localized in sp^3 matrix of 1-10 μm overall size is different from that of sp^2 clusters in a quantum sized particle of 1-10 nm. In the former case the localization is constrained with the sp^3 matrix where the edge effects can be largely ignored. This is in clear contrast to the latter case where the edge effects are as prominent as the surrounding sp^3 matrix.

QY can be calculated by comparing the integral intensity with constant absorbance.[109] If we take a look at the QY of the GO, it is relatively low (6.9 % Ref.[40]) at times as low as less than 1% [38] which can be because of two factors.[81] The presence of (i) isolated sp^2 domains and (ii) reactive sites such as the epoxide groups inducing nonradiative recombination. It is expected when the surface is modified, the reactive sites may be passivated and hence luminescence yield may improve. Defect states within the interfaces may cause nonradiative transition, which might reduce the emission intensity [125] and thus the QY. In some cases no emission is observed until GO was subjected to specific modifications such as appropriate control of the sp^2 cluster concentration,[36] or surface passivation of the reactive sites.[89]

3.5 Doping

Similar to regular semiconductors [16,21] GO is subjected to doping. In this section we will discuss the effects of substitutional doping while that of surface electron transfer [126,127] will be discussed latter. Doping of GO is rather interesting and extensively investigated [99,128,129] especially with nitrogen,[99,129] boron,[128] halogens [130] etc. In the context of fluorine doping, a completely fluorinated graphene behaves as a thinnest insulator and the only stable stoichiometric graphene halide (C_1X_1).[130] Fluorine-doped rGO is reportedly a better substrate for surface enhanced Raman spectroscopy than unmodified rGO. Since F doped rGO or GO doesn't show any emission, we will not discuss their details. However, the reader is advised to refer to a recent review by Karlicky et al.[130] In the process of doping, formation of other phases is an important issue. For example, B doping has resulted in the presence of B_4C, B_C, BC_2O, BCO_2 and B_2O_3.[128] Recently, energy-level structure of N-doped GO QDs is discussed.[129] Simultaneous doping of B and N doping is also possible, where GO is converted into boron carbonitride by substitutional doping.[131] Interestingly, after the doping process (at 900° C), a significant amount of oxygen content in the GO is evidenced from XPS. Essentially BN phase is formed within GO matrix, *c.f.* boron doping and secondary phase formation.

Going into the details, a study on N doped GO QDs has revealed vital findings where nitrogen atom creates an intermediate state (Figure 8).[129] Note that in Ref.[129] the authors refer GO QDs as graphene QDs while significant quantity of oxygen is evidenced from XPS and EELS. For a suitable illumination, the following transitions are possible, where the wavelength equivalent is given in the brackets for each of them. 6.1 eV: π →π*of C=C (202 nm), 4.6 eV: π →π*of C=N (274 nm) and 4.1 eV: π →π* C=O (302 nm), see Figure 8.

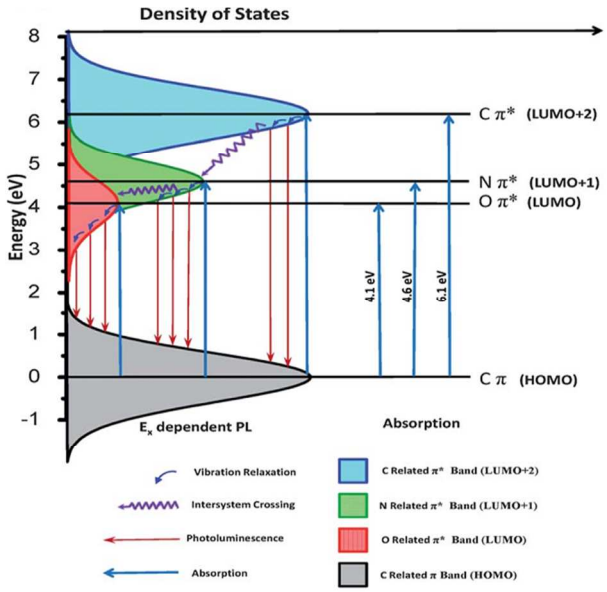

Fig. 8 A schematic diagram illustrating the energy levels of the nitrogen doped GO QDs. Reproduced with permission from Ref. [129]

Tang et al.[129] suggested two methods of recombination of excited *e/h* pairs. (i) Direct recombination after vibration relaxation, producing fluorescence and (ii) C π* →N π* and N π* → O π*, followed by vibration relaxation and finally radiative recombination. Process (ii) occurs because of the nitrogen doping via intersystem crossing.[129] The interpretation of emission from GO is based on the involvement of oxygeneous functional groups in contrast to sp^2 localization. Significant enhancement of blue emission was achieved after doping rGO with nitrogen (2.3–4.7 at%) via thermal annealing in the presence of ammonia gas for different time periods.[99] During this process, formation of graphitic carbon nitride (C_3N_4) in α and β phases was also detected. These phases impose significant changes in the emission and electronic properties. The emission mechanism is explained in Ref.[99] is based on localization of sp^2 clusters.[36]

A typical emission spectrum from boron doped GO is shown in Figure 9. The emission is attributed to the recombination of *e/h* pairs within the electronic band gaps of sp^2 clusters [71,93,94] including the effects from size, shape and fraction.[36] The fluorescence spectrum of as synthesized GO consists of three components centered at 520, 716, and 827 nm, while the size of sp^2 clusters increased to 6.90 nm after B-doping. Despite of the increase in the sp^2 cluster size the green emission peak is blue shifted (to 494 nm) as compared to that of annealed GO with a decrease in its intensity. The second peak at ~636 nm is attributed to the boron carbide phase ($B_{4.23}C$ emits ~795 nm Ref.[132], $B_{4.3}C$, $B_{6.5}C$, and $B_{10}C$ emit > 595 nm Ref.[133]).

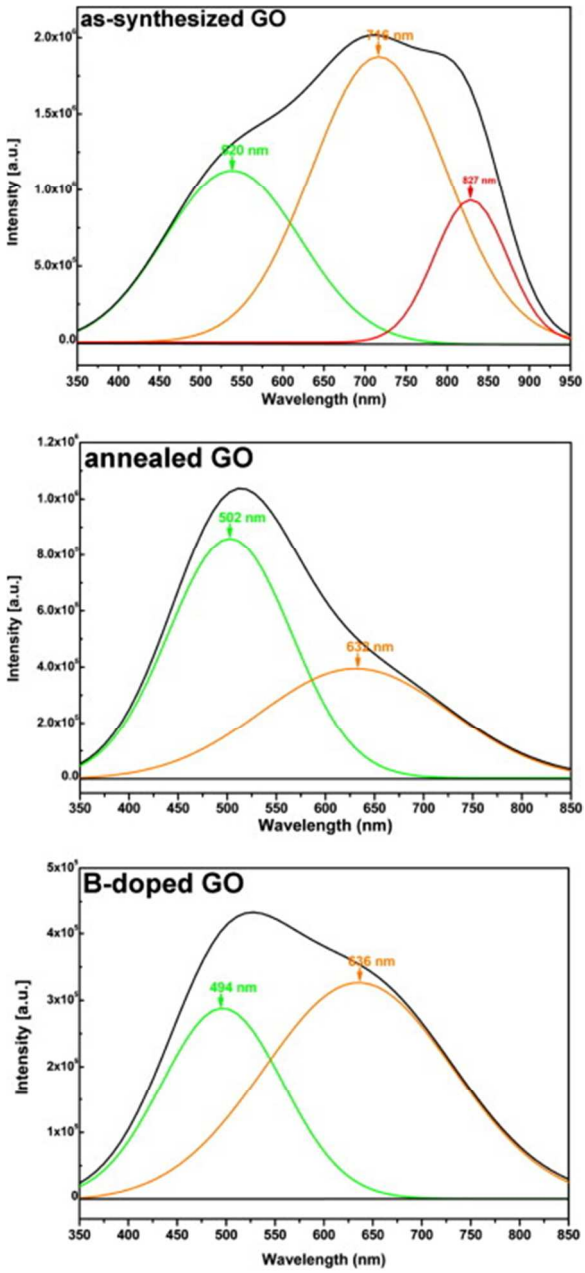

Fig. 9 Emission spectra of as-synthesized GO, annealed GO, and B-doped GO. Reproduced with permission from Ref.[128]

3.6 Covalent modification

In the previous section we have seen substitutional doping and its effects on emission properties of GO and r GO. In this section, we will see the variations in optical properties when GO or rGO were covalently functionalized with various moieties. The covalent functionalization is facilitated through the surface functional groups of GO or rGO. In this direction, researchers have studied considerable types of modifications aiming at various applications [81,134] including nonlinear optical properties.[135-137] Typical modifications are surface passivation of the reactive sites,[89] chemical bonding with fluorescent ions [90] etc. The covalent modification has various advantages such as improved solubility in intermediate organic solvents, coupling with other functional materials where the spacer length can be tuned and the quantity of loading can be increased. In a typical example, the functionalization can take loading as high 5 wt% of dye.[79]

In an approach shown recently [79] the covalent attachment to GO does not alter the absorption and emission properties of the dye. On the other hand the pH sensing capability is achieved through amidic group via reversible protonation. GO layers were functionalized with azo-pyridine [81] at an interlayer separation of 0.9 nm showing a bright blue emission via excited ESIPT. The fluorescence spectrum (λ_{ex} = 416 nm) of the GO solution (QY = 0.03 %) depicted a broad peak at ~560 nm.[138-140] This peak is blue shifted to 470 nm for the GO–azopyridine (QY = 8 %) and the intensity increases 400% with respect to GO. Basically, functionalization not only creates but also enhances the luminescent centers in the composite. The enhanced optical emission is because of ESIPT between the –OH group (alpha) of the phenol moiety and the azo group. This is similar to substituted hydroxyl benzaldehydes where the emission is due to keto (H) form and enol-Azo form ESIPT.[141]

The covalent functionalization of GO with anthryl moieties is interesting.[134] The emission properties of 2-aminoanthracene (pale yellow under daylight, cyan (491 nm) under 365 nm) were significantly changed when functionalized with GO (dark red under daylight, blue (400 nm) under 365 nm). This leaves us with a shift of ~91 nm. Such a large shift is simply attributed to the interaction between the anthryl moieties and GO, however, the shift is almost absent when the components are physically mixed. Hence the interaction between π-orbitals is insignificant for the shift. Hence a deeper investigation is required to explain how an unconjugated covalent bond causes such shift.

Chemical bonding with fluorescent ions such as Mn^{2+} has shown interesting results.[90] The authors attribute emission from rGO to the π-π* transitions due to localization while resonance energy transfer takes place from Mn^{2+} ion to π* states of rGO (Figure 10).[90] In this hybrid, Mn ions are bonded to the carboxyl groups of rGO which places the ion in the close proximity of sp^2 cluster. Finally the authors note that the emission from GO is enhanced.

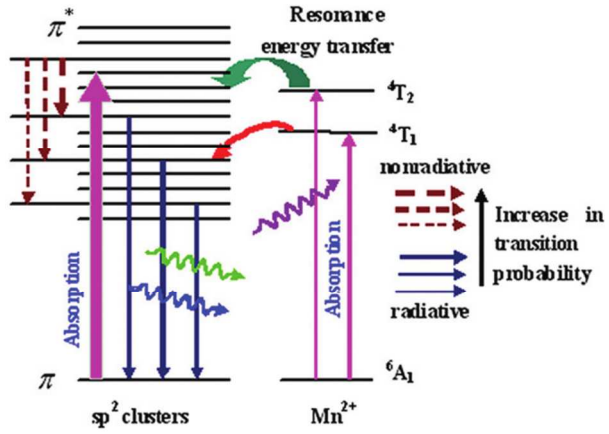

Fig. 10 (Color online) Schematic mechanism of fluorescence from the Mn^{2+}-bonded rGO where solid and dotted lines representing the radiative and nonradiative relaxation processes, respectively. Reproduced with permission from Ref. [90]

4. Nonlinear optical response

In principle GO can be a more suitable material for optical limiting applications than Gra because of the tunable energy gap. It would be appropriate to briefly describe some unique nonlinear optical features depicted by GO. By definition, nonlinear property is that the transmission decreases with increasing light intensity (good linear absorption at low input levels). This feature is extremely useful for eye protection where a broadband (visible to IR if possible) optical limiter is demanded. Nonlinear response of GO is different from that of the other carbon allotropes while similar to organic materials.[142] In the case of GO, for picosecond pulses two-photon absorption is predominant, while for nanosecond pulses excited state nonlinearities play a vital role.[142] Although Gra is considered for such applications,[6] GO has its own advantages such as 2D nature and more importantly its functionalizability. The functionalizability allows covalent bonding of organic dye molecules (see Section 3.6) or other complementary optical materials and composites.[143,144] Interestingly, GO depicts better optical limiting response than fullerene (C_{60}) as shown by various groups.[145,146] Experimentally it is evidenced that covalent functionalization with C_{60},[135] porphyrin,[135,136] or oligothiophene [137] improves the nonlinear optical performance in nanosecond region. These studies suggest that the hybrid materials have better nonlinear absorption via photoinduced electron or energy transfer. Fluorinated GO has shown higher nonlinear absorption, nonlinear scattering and optical limiting threshold which are about an order of magnitude better than GO.[147]

5. Ionic interactions

In the earlier sections we have seen that the functional groups on the GO may be one of the causes for the emission where they open the band gap of graphite. These functional groups are mainly oxygen-contained, which are prone to external interferences such as ions (cations and/or anions). In the following we will discuss the emission dependent on H^+ (pH) and other ionic species in two different subsections.

5.1 pH dependent optical emission

Essentially, the Fermi level of GO is shifted depending on the pH values where the electronic structure of GO is manipulated. As a result different emission colors are noticed.[69] Note that this is in contrast to GO-azo pyridine composite, where the increased symmetry of the π–π* state decreases the Franck–Condon factor. Consequently radiationless decay is decreased, thereby the fluorescence from such composites gets brighter with decrease in pH.[81] Blue fluorescence from GO QDs is found to be pH-dependent where they were derived from cleaving CNT possessing zigzag sites.[37] The suggested mechanism hinges on the protonation of the emissive zigzag sites where their ground state is $\sigma^1\pi^1$. The fluorescence can be recovered when deprotonated (alkaline conditions). Multicolour fluorescent GO was synthesized by cleaving CNT upon oxidation [69] while the fluorescence depicted bathochromic shift [148] which was attributed to deprotonation of –OH and –COOH groups.[149,150] It is also notable that ionic-liquid-assisted electrochemical exfoliation showed similar results.[151] The intensity of the emission from azo-pyridine functionalized GO [81] can be controlled by adjusting the pH value. In this case the radiatiave surface defects are passivated.[149,152] The intensity changes are because of the protonation and deprotonation of the functional groups which may cause electrostatic doping (i.e. shift of Fermi level as seen in the case of carboxylate SWNTs [153]). Interestingly, this is in contrast to the fluorescence of GO QDs with change in pH where the intensity of fluorescence decreases with decreasing pH (13 to 1).[37] In a study by Peng et al.[112] the GO QDs emit strong fluorescence under alkaline conditions. While in acidic conditions the fluorescence is quenched because of the protonated free zigzag sites.

5.2 Other ionic species

Since GO QDs consists of oxygen containing functional groups they can act as sensing platform when interacting with ions. *c.f.* protons in the case of pH. The variation in the emission intensity is related to the molecular interaction. The quenching occurs because of inner filter effects, creation of non-radiative paths, electron transfer process and ion binding interactions.[154] In this section we will see two types of effects because of ionic interactions. (i) The quenching of fluorescence by itself in the presence of guest ions and (ii) quenching the fluorescence of other materials.

Generally quenching of fluorescence of host in the presence of guest ions takes place through collisional or dynamic quenching. Stern-Volmer equation [155] describes the dynamic and collisional quenching via $F_0/F = \tau_0/\tau = 1 + k_q\tau_0[Q]$, where F_0 and F are the fluorescence intensities before and after the arrival of guests, respectively. k_q is the rate constant of dynamic (collisional) quenching; τ_0 and τ are lifetimes of fluorophore before and after the arrival of guest ions, respectively; [Q] is the concentration of the guest ions in the solution. In the context of static quenching, a non-fluorescent complex forms between the host and guest and as a result the life-time of the fluorophore is unperturbed, i.e. $\tau_0/\tau = 1$. Now, the $k_q\tau_0$ is called as association constant.[155]

GO QDs were employed as selective ion sensing materials where the quenching of fluorescence was observed (inversely proportional) under the influence of Cu^{2+}.[28] The intensity was linearly decreasing within the range of 0-15 μM of Cu^{2+} ions with a maximum detection limit of 0.226 μM. Authors also suggest that the quenching mechanism is predominantly static in nature as described by Stern-Volmer equation.[28] The interaction with P^- and P^+ was studied with Au NPs and GO separately by Mamidala et al.[91] Various combinations were shown in Figure 11a and b. We can see the quenching of emission at 640 nm from GO+P^+ complex in contrast to GO+P^- complex. This indicates that the interacting donor-acceptor complexes are formed between opposite charges. The quenching is attributed to photoinduced electron or/and energy transfer.[156] This interaction is also reflected in the fluorescence lifetimes (Figure 11c and d and Table 1 for the time scales). On the other hand, in the case of positively charged picket-fence porphyrin the interaction is attributed to π-π type.[157]

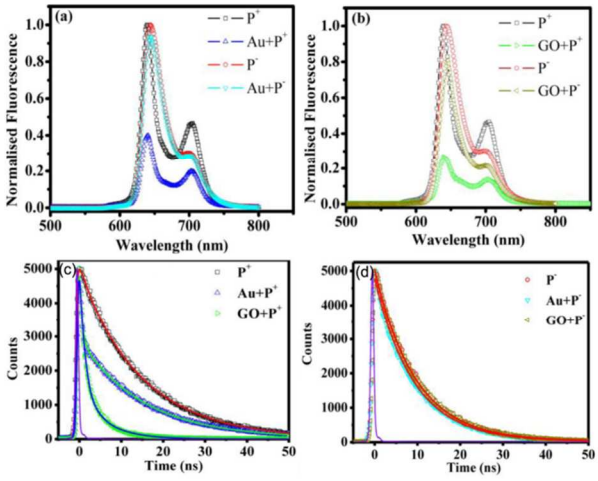

Fig. 11 (Color online) Spectra of P^+, P^-, $Au+P^+$, $Au+P^-$, $GO+P^+$ or $GO+P^-$ in water dispersion (a) and (b) fluorescence, λ_{ex}= 430 nm. (c) and (d) decay curves. The instrument response function is shown in violet color trace. Figure reproduced with permission from Ref.[91]

Previously, interaction of GO with charged porphyrin,[91] is discussed; similarly Eu^{3+} ions are also a subject of investigation against the fluorescence from rGO (Figure 12).[158] In this study, the authors referred rGO as graphene as it contains very low percentage of oxygen. Nevertheless, the complexation requires oxygen functionalities on gaphene, hence, we will be referring this as rGO instead of graphene. This complex is shown to quench the fluorescence of Rhodamine-B dye while the complex of Eu^{3+}/rGO being active (λ_{ex} = 314 nm, λ_{em} = 614 and 618 nm). Note that the various oxygeneous functional groups on rGO are spatially distributed around the Eu^{3+} ion should be at low symmetry sites.[159] This is in contrast to an earlier explanation,[90] where an energy transfer takes place from Mn^{2+} to the localized states of sp^2 on rGO. In this case the involvement of oxygen containing functional groups can be avoided, despite of the covalent bond between rGO and Mn^{2+} (see Section 3.6 and Figure 10). Also see anthryl functionalized GO and its emission properties [134] in Section 3.6. In the PLE spectrum (Figure 12) the interacting oxygen functionalities and Eu^{3+} have shown a strong band at 314 nm [160,161] while the other five peaks are attributed to f-f transitions of the Eu^{3+} ions. The authors suggest triple-exponential decay (average lifetime ~391.13 μs) due to the differences in the ligand environments in the rGO around Eu^{3+}. The combination of GO is not limited to Eu^{3+} but extends to europium oxide.[162]

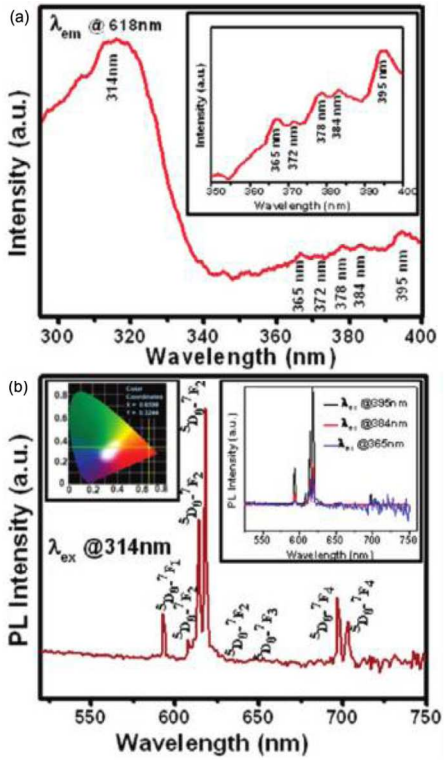

Fig. 12 (Color online) (a) fluorescence excitation spectrum of the rGO and Eu^{3+} complex, inset 350-400 nm region, and (b) Fluorescence spectrum (λ_{ex} = 314 nm). The right inset shows the other three distinct emission spectra at different λ_{ex} and the left inset shows the color coordinates (x = ~0.66 and y = ~0.32). Reproduced with permission from Ref.[158]

6. π-π type interactions

Moving onto the combinations with organic semiconductors, Yang et al.[163] studied fluorescence from GO-P3HT nanocomposite heterostructure and suggested a π–π interaction between the two components.[164-166] In this heterostructure P3HT chains are attached to rGO while the former coats a thin-layer on the latter. Later in 2012, PDS and pump–probe techniques are employed on GO–P3HT layer-to-layer hybrid and results support the earlier argument of π–π interaction (Figure 13).[92] In solution phase, the normalized PL spectra of P3HT, GO–P3HT and rGO–P3HT are of comparable intensity (Figure 13a), with small differences in the range 540–600 nm, see inset. In contrast to this, in the solid phase the presence of GO or rGO has significantly quenched the emission from P3HT (Figure 13b) via π–π (weak Coulombic) interactions. See Table 1 and Figure 13c for decay times and measurements, respectively. Furthermore the transient response studies (650 nm, Figure 13d)

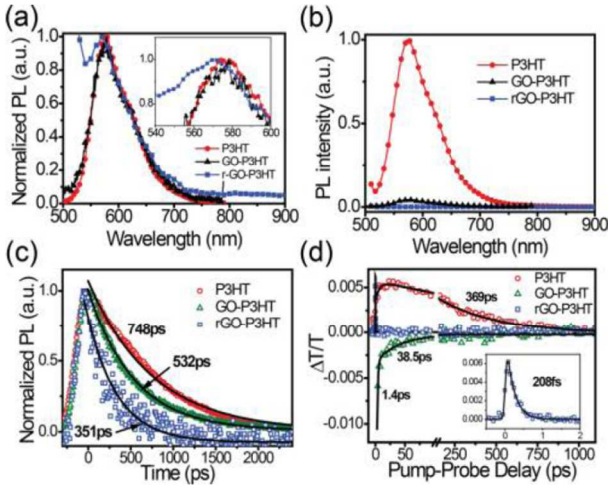

Fig. 13 (Color online) (a) normalized fluorescence spectra, (b) fluorescence intensity while P3HT is 0.1 mg/mL, (c) TCSPC decay curves and (d) relative changes in transmission for varying pump (10 μJ/cm^2) –probe delays; λ_{ex} = 400 nm and λ_{em} = 650 nm. The inset shows the magnified spectrum of rGO–P3HT in the first 2 ps. All cases are dispersion in $CHCl_3$. Reproduced with permission from Ref.[92]

indicated that GO–P3HT composite did not show any stimulated emission. However photoinduced absorption signal with two decay times (τ = 1.4 and 38.5 ps) is observed in contrast to pure P3HT which depicted stimulated emission. As a result, an ultrafast charge dissociation of P3HT excitons [167] takes place at the interface and charge pairs are injected into GO as fast as 1.4 ps. In the case of rGO-P3HT the electrons generated in P3HT are injected rapidly into rGO. In this context both GO and rGO are very useful in solar cells where fast transfer of photogenerated charge is the primary objective.[168] In the case of covalent functionalization between P3HT and GO [169] the overall fluorescence quenching includes dynamic quenching and forms a non-fluorescent ground-state complex.[169] Also this π–π interaction blue shifted (~4 nm) the absorption maximum of P3HT. It would be more conclusive if the XRD patterns were investigated on solid samples, where the consequence of π-π interaction and layer formation can be understood rather precisely via (002) interplanar spacing of GO.

It is important to note that the case with PANI is not similar to P3HT or even inorganic semiconductors. When graphene is combined with PANI either through *in situ* polymerization or mixing [170] the emission properties of PANI were preserved suggesting an inappropriate band alignment and possible π-π interaction.

The fluorescence from rGO and its decay life time were enhanced with Rb [70] through non-covalent bonding. Apart from preserving the native features of rGO such as excitation dependent fluorescence, a slight shift in the peak position is observed. From the fluorescence decay (Table 1) it is suggested that the shorter component has higher contribution (~84%).[58,87] Other study on π-π interactions of rGO with positively charged picket-fence porphyrin [157] suggested a quenching of fluorescence from porphyrin under the influence of rGO.

7. Heterointerfaces

7.1 Photovoltaics

GO and rGO are proven to be potential in photovoltaic applications. For example, the hole transport property of PEDOT:PSS can be improved with the addition of GO at a suitable concentration.[9] Furthermore such combinations can yield a band gap larger than 1.1 eV for 10-15 wt% of GO, while the carrier transport property is majorly determined by the fine structure of host PEDOT:PSS.[171] At a certain concentration, GO in dye-sensitized solar cells acts as an electron collector and transporter resulting in an enhanced photovoltaic performance.[172] Moreover it also improves the transfer of electrons from the films to the FTO substrate.[173] In contrast to this, partially reduced GO is employed as an active layer and rGO is employed as electron and hole collecting layers. This symmetric device configuration is shown in Figure 14a. The device has depicted a V_{oc} of 0.017 V-0.014 V. However the authors in Ref.[174] did not present any fluorescence data from partially reduced GO and rGO in case if there is any.[15,36,58] Despite, this study is remarkable where it employs rGO as an active material in the device. Although the fluorescence from rGO is debatable, however, the energetic states and their alignment can be deduced by fabricating *pn*-junctions.[18] Such studies can unveil the information about charge generation and subsequent separation. Composite HJs were studied for electrical characteristics where they can be integrated into the well established silicon devices.[171] The authors have studied carrier transport in crystalline-Si (100) (c-Si)/conductive PEDOT:PSS composite HJs.[171] See Figure 14b for the band diagram under a small FB. The results suggest that the carrier transport mechanism is changed from diffusion to the space-charge recombination with the increase of GO content in PEDOT:PSS. Upon introducing GO in PEDOT:PSS apart from the improvement in the ideality factor (GO-PEDOT:PSS-2.91 PEDOT:PSS-1.12) the efficiency of the device is enhanced.[171] The cell characteristics are η = ~10.3 %, J_{sc} = 28.9 mA/cm^2, V_{oc} = 0.548 V and FF = 0.675 at a GO content of 12.5 wt% with diffusion and recombination in the space-charge region. Improvements in charge extraction efficiency and reduced charge recombination were observed by inserting rGO–TiO_2 composite layer as optical spacer between the active layer and Al electrode.[175] This interfacial layer blocks the holes as well. As a result the PCE is ~4.18 % and ~5.33 % for TiO_2 and rGO–TiO_2 interfacial layer, respectively where a similar structure without the interfacial layer has shown a value of ~3.26 %. It is obvious that defects of GO or rGO influence the device performance. However, in an interesting study by Chang et al. [176] the defects and atomic structure is controlled yielding well regulated infrared PR (responsivity of ~0.7 A/W) in rGO phototransistors. This study evidenced that the PR is mostly dependent on oxygenous defects. Furthermore external quantum efficiency of ~97% and no PR degradation even after 1000 bending cycles are significant.

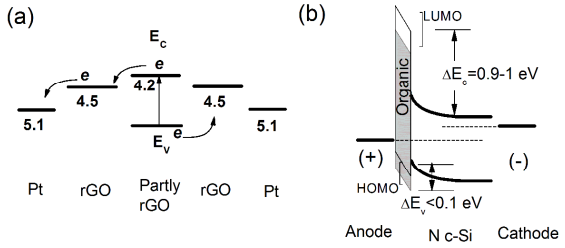

Fig. 14 (Color online) (a) Schematic energy level diagrams (b) the band diagram of the crystalline silicon (N c-Si) and PEDOT:PSS/GO composite junction under small FB. Figure redrawn based on Refs.[171,174]

7.2 Nanocomposites

Nanocomposites are very potential materials in scientific and technological applications in which rGO or GO is employed extensively. The host matrices are inorganic or organic in nature depending on the type of application. Inorganic matrices can be CdSe nanoparticles,[177] ZnO@ZnS hollow dumbbells,[29] zinc (hydr) oxide,[178] TiO_2,[77,179,180] Fe- doped TiO_2 nanowires,[181] noble metal doped TiO_2,[182] ZnO,[180,183,184] Ag/ZnO,[185,186] ZnS,[187] CdS,[188-191] Ta_2O_5,[180] CdSe,[177,192] CdTe,[193] Ag_2Se [194] etc. Examples of organic components include PANI,[170,195] P3HT,[163] methylcellulose [143] etc. In this section we will focus on the optical properties of these material combinations in the context of charge transfer, where the relative position of HOMO and LUMO levels play a crucial role.

When CdSe NPs were composited with rGO [177] the PL from CdSe is observed to decrease and apart from an enhancement in the PR. This indicates that the photoinduced carriers from the

CdSe NPs can be transferred to the rGO effectively. Recent investigation [196] on ZnO and GO QDs presents important insights in the emission (Figure 15a) from a composite with an application in LEDs. The MO levels, DOS for pristine and G–O with epoxy bond (G–O_{epoxy}) including the oxygen PDOS are shown in Figure 15b. The results indicate that there are significant orbital hybridizations after the chemical bond with the oxygen atom. The mechanism of emission is shown in Figure 15c. Under illumination the photo-excited electrons from the O2*p* of the ZnO are transferred to the unoccupied states of G–O_{epoxy}. Then these electrons recombine with the holes in VB of ZnO creating two additional peaks in the spectrum. Such transitions are determined by the selection rule ($\Delta l = \pm 1$), i.e. l = 0 or l = 2 electrons can recombine with O2*p* (l = 1). Contextually, DFT results suggest that only *p* orbitals contribute to the LUMO level of pristine graphene and hence no transitions as l=1 and the un-hybridized LUMO level splits into three levels with oxygen attachment (LUMO, LUMO+1 and LUMO+2). See Figure 15c for various allowed transitions. The emission from ZnO-GO QDs is deconvoluted into four Lorentzian peaks centred at 379 (band to band), 406 (LUMO+2 in G–O_{epoxy} to VB of ZnO), 436 (LUMO in G–O_{epoxy} to VB of ZnO) and 550 nm (V_O or Zn_i), according to the authors' attribution.

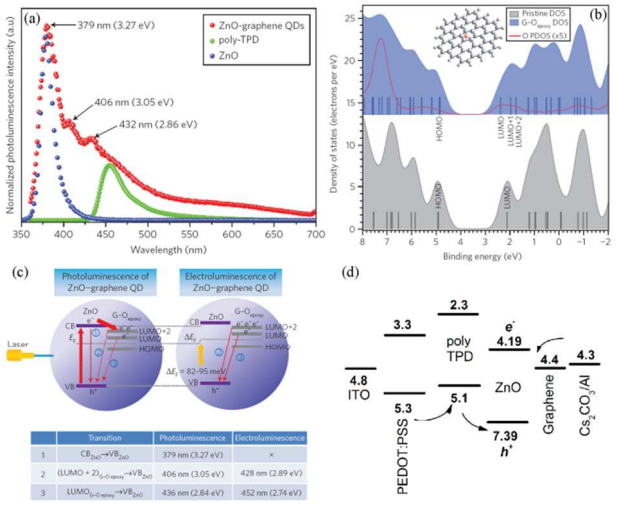

Fig. 15 (Color online) (a) emission spectra, (b) DOS of graphene and the G–O_{epoxy} model. MO energy is indicated with vertical bars in each calculated DOS. Inset: G–O_{epoxy} model, (c) PL and EL transition scheme for ZnO–GO QDs, (d) band alignment of various components in the LED. Parts (a), (b) and (c) are reproduced with permission from Ref.[196] Part (d) is redrawn based on Ref.[196]

Optical and electrochemical properties of ZnO nanowires/GO heterostructures reveal that GO can suppress surface states of ZnO enhancing the UV-emission of ZnO.[197] This enhancement is a balance against the green emission, which is due to V_Os in ZnO as widely accepted,[16-18] also see cross references in Ref.[17] There is also a possibility that the electrons are transferred to GO due to the energy level alignment (Figure 16a). Of course, GO can perhaps passivate the surface [198] in which case ionized V_Os can be suppressed, thereby enhancing the UV emission. Similar case can be seen in the literature,[199] in which the authors compared PL properties of ZnO nanorods when coated with GO and rGO. Notably, the emission due to interband transition is enhanced when ZnO nanorods were coated with rGO (Figure 16a). In another example of GO-ZnO composite,[183] the green emission (centered at ~550 nm) from ZnO was blue shifted (0.15 eV) and quenched upon compositing with GO. The authors suggest additional pathways for the subdued emission via interfacial charge transfer from ZnO to GO.[200] In Ref.[200] the authors show that the PL quenching increases with increasing the concentration of GO without any shift in PL peak position. This might be because of the preparation technique that is used. It is notable that the electrons from the ZnO were primarily used in the reduction of GO to rGO upon irradiation of UV light. In contrast, to Ref.[200] Singh et.al.[183] eliminated the electron transfer from ZnO to GO via modifying the preparation method. It is also suggested interaction is similar to SnO_2–CNT or ZnO–SWNT composites.[201] Although the suppression of V_O's is explicit the mechanism behind such passivation and the creation of additional path ways should be studied further. On the other hand the fluorescence from GO is also seen to quench [202] when combined with ZnO.[184]

Mott-Schottky plots (Figure 16b) provide information about the feasibility of transfer of photogenerated electrons to rGO.[203] In the case of CdS nanoparticles, it is thermodynamically permissible for the absorbed O_2 to produce superoxide radicals ($\cdot O_2^-$) under visible light illumination. The photoinduced electrons are transferred to rGO delaying the recombination process.[203] Similar to the earlier cases the PL intensity from CdS is subdued.[190,204] By considering the energetic locations [205] of CdS (χ_{CdS} = 4.00 eV) and rGO (E_F = 4.42eV), under suitable illumination electron transfer from the CB of CdS to rGO and hence the emission is quenched (inset of Figure 16b).

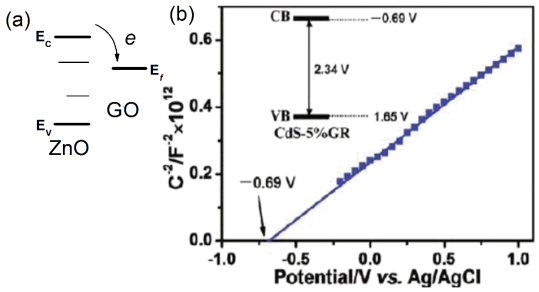

Fig. 16 (Color online) Schematic diagram of the electron transfer between ZnO NWs and GO films and (b) Mott-Schottky plot for the CdS-5% rGO nanocomposite in 0.2 M Na_2SO_4 aqueous solution (pH = 6.8), reproduced with permission from Ref.[203]

The fluorescent spectra from GO grafted CdTe (exciton band at 520 nm) are shown in Figure 17.[193] The emission is centred at ~540 nm under 365 nm illumination. In the case of GO-Cl, the sample has shown some visible fluorescence may be due to sulfonyl chlorination of the GO. As seen earlier, although GO is itself fluorescent it can quench the luminescence of other materials.[188,206,207] GO quenched the interband transition (due to fluorescence resonance energy transfer, or nonradiative dipole–dipole coupling between CdTe and GO [208]) and depicted an emission around 420-450 nm. This is because of the amidation process

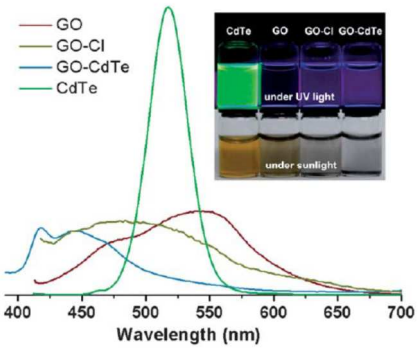

Fig. 17 (Color online) Fluorescence spectra, λ_{ex}= 365 nm. The inset shows the optical images λ_{ex}= 365 nm (top) and under λ_{ex}= sunlight (bottom). Reproduced with permission from Ref.[193]

which creates localized sp^2 clusters and structural defects.[15,39] This is similar to CdSe nanocrystals (cubic and hexagonal) where the PL from CdSe is quenched by rGO.[192]

TiO_2 and GO alternative layer structure is studied [77] for luminescence properties and decay life times. The emission properties and band diagram (ignoring the presence of any defect-related [58] states) are shown in Figure 18. For TiO_2 case the emission peak (at ~600 nm) is red shifted (~650 nm) significantly upon increasing the λ_{ex} which is attributed to vacancy related defects [209-211] within the band gap. The QY is as low as <1% [210] (Figure 18c) with a lifetime component that is only a little longer than the ~250 ps resolution. In the case of GO/TiO_2, 550 nm band is blue shifted (to ~500 nm) while the emission is subdued for rGO/TiO_2 case. Authors attribute this blue-shift to the quenching effect, which is more effective on the longer wavelength side of the PL spectrum of TiO_2.[211] The quenching effect creates non-radiative decay channels and hence a faster PL decay should be noticed. The present decay curves suggest that the fluorescence quenching effect plays a minor role in blue shift. However, the authors attribute the emission to IOT between TiO_2 and the localized sp^2 domains of GO in a charge-separated configuration. From Figure 18d, the electrons localize in the CB of TiO_2 while the holes can either relax to the defect level or injected into the O 2*p* level for both λ_{ex}. The optical recombination of electrons from CB of TiO_2 with that of holes in O2*p* levels of GO is allowed (reduced symmetry at the interface [104]). This is seen as the blue-shifted emission (type-II fluorescence [105]) for both GO/TiO_2 and rGO/TiO_2 cases. Such recombination occurs due to the intimate contact between the components. In the present case the typical distances are ~1.608 nm (GO/TiO_2) and ~1.156 nm (rGO/TiO_2).[212] The longer PL decay time of GO/TiO_2 is attributed to the reduced overlap of electron and hole wave functions.[105] In the rGO/TiO_2 case the intimacy between TiO_2 and rGO increased and hence the inter-connectivity of localized sp^2 sites and the percentage of zero gap regions is also increased.[36] This leads to enhanced charge transfer and consequently better quenching of PL with shortened lifetime.[36] As the oxygen content decreases the O2*p* level will be lifted up causing a red shift in the PL peak of rGO/TiO_2 relative to that of GO/TiO_2. It is notable that the decay times of TiO_2 and rGO or GO were not in the same order of magnitude and as a result, the composite decay time is an integral effect of their individual characteristics. If one has to consider such an argument, then a way to be figured out to resolve the decay constant for each of the components. It is interesting to see that the above interpretation combines the effects of sp^2 cluster localization and the involvement of O 2*p* level.

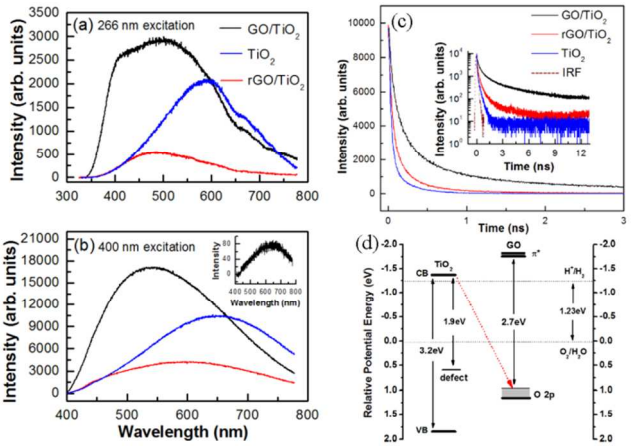

Fig. 18 (Color online) Emission spectra λ_{ex} is (a) 266 nm and (b) 400 nm. The inset of (b) shows the fluorescence spectrum of as synthesized GO, λ_{ex} = 400 nm. (c) PL decay curves, λ_{ex} = 400 nm, inset: 0 to 12 ns on a log scale. The fluorescence signal was collected over the entire spectrum of each sample. IRF: instrument response function and (d) schematic of band diagram for TiO_2 and GO, water oxidation potential is set at 0 eV. The dotted arrow red line marks the IOT. Figures are rearranged and reproduced with permission from Ref. [77]

The interface between Fe-doped TiO_2 and GO enables transfer of electrons from the CB of the semiconductor to GO (Figure 19a) quenching the overall emission. However Fe-doping enables the creation of *e/h* pairs under visible light illumination. Similar study can be seen on the suppression of PL from TiO_2 under the influence of GO.[179] Furthermore, PL measurements on GO–ZnS nanocomposite suggest that graphene can be employed to quench the defect level emission.[191] However, the details of the defect levels and their passivation mechanism were not suggested. Although it is accepted that the defect levels can be passivated variously with polymers or other inorganic coatings,[198] the energetic location of the defect and its alignment with the bands of GO is very important factor to consider. We can see other examples in which electron transfer takes place from TiO_2 to GO and rGO.[182] Other inorganic low band gap semiconductor such as Cu_2O showed similar effect in terms of transfer of photogenerated charge carriers (Cu_2O/PA/rGO and Cu_2O/rGO).[187] Furthermore the transfer of electrons and/or holes takes place across the interface even if more than one semiconductor is present. It is the case with ZnO@ZnS hollow dumbbells–GO composite,[29] see the schematic charge transfer process in Figure 19b.

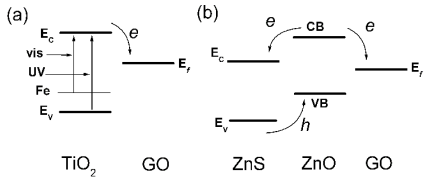

Fig. 19 (a) The interface between Fe-doped TiO_2 and GO (b) the band alignment of ZnO@ZnS hollow dumbbells-graphene composites.[29] Figures redrawn based on Refs.[29,181]

Fluorescence quenching ability of GO is extended to fluorescein moieties (fluorescein derived silyl ether) [213] similar to other complexes with organic dyes.[136,214] The fluorescence quenching is explained based on the band alignments of fluorescein and GO.[215] This allows the transfer of photogenerted electrons into the CB of GO (Figure 20). Besides the regeneration of fluorescein is facilitated by I_3^-/I^-.

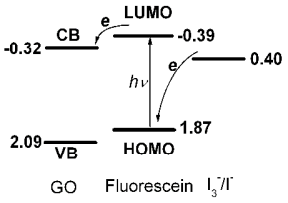

Fig. 20 The energy level diagram illustrating the electron transfer process between GO and fluorescein moiety in fluorescein derived silyl ether. Figure redrawn based on Ref.[213]

8. Conclusion and outlook

In this review we have focused on the optical properties of GO and rGO where the fluorescence properties are explored recently. We have discussed the existing mechanisms and pointed out largely ignored issues such as self-rolling, byproduct formation, concentration, dielectric constant etc. It is important to note that the emission properties of GO depends on the synthesis process. The distribution of various oxygen containing functional groups is completely process dependent. By given the vast amount of literature, a simple and versatile quantification technique is demanding to quantify the functional groups and their spatial distribution. These two factors play a crucial role in determining the emission properties. Generally, ensemble of GO sheets is considered for spectral analysis. This ensemble includes various shapes, sizes which are crucial parameters to be evaluated. In case if the sample contains a class of material at low concentration with high QY, then we may observe a predominant emission peak. While that peak wavelength will be interpreted against the majority distribution. In order to avoid such discrepancies one need to consider studying single sheet of GO and its fluorescence. Notably, the degree of oxidation and reduction can be employed to tune the emission properties of GO and rGO while a precise control on the relative densities of functional groups still needs to be achieved. For example, during the reduction some of the functional groups are reduced faster than others, although the optical band gap is tunable. The detailed understanding of nanometer- to sub-nanometer-scale structures of GO and rGO can perhaps show new directions for the interpretation of their fluorescence. The plus point is that the oxygen containing functional groups on GO and rGO enables further functionalization with other materials. Moreover, it is soluble in a variety of solvents and hence subsequent incorporation into composites is an easy task.

Fluorescence from GO opens new and exciting opportunities for exploration of photonic devices such as LEDs, photodetectors, photovoltaics etc. However, photodetector studies should focus on wavelength selectivity.[18] Such studies not only give further insight into the energy levels of GO but also shed some light into the fluorescence mechanism in an indirect fashion. The fluorescence from GO and rGO depend on various factors. Despite, molecular sensing with rGO is quite promising, where its sensitivity to certain chemicals and relatively higher signal-to-noise ratio are worth mentioning. Although there are some *in vivo* studies, cell imaging etc, for practical applications the selectivity to some ions or molecules and recycling require further studies.

The characteristics of GO and rGO are not alone determined by the level of oxidation, but also strongly influenced by the distribution of conjugated carbons, holes, vacancies, folds, wrinkles, interfaces of sheets etc. Furthermore one should note the differences in the emission depending on the synthesis process.[15,36,58] Strong localization of sp^2 clusters and involvement of oxygen functional groups in the fluorescence of GO or rGO deserves further attention. If the oxygen functional groups have to be eliminated from the luminescence mechanism, then the sp^2 clusters should be localized in a matrix that doesn't contain any oxygen or related functional groups. For example, a complete substitution of oxygen with a suitable element while retaining the lattice constant of oxidized (modified) graphene can be an example target material. Also the average sheet dimensions should not be modified in the process of substitution. This is in clear contrast to a simple reduction of GO. The unique 2D lattices of GO and rGO provide an exciting platform in which various applications and fundamental interests are involved in engineering, physics, chemistry, biology and materials science.

9. Abbreviations

Materials
P^- negatively charged porphyrin
P^+ positively charged porphyrin
CNT-Carbon nanotube
Au NPs-Au nanoparticles
PEDOT:PSS- Poly(3,4-ethylenedioxythiophene) Polystyrene sulfonate
Poly-TPD- poly(N,N′-bis(4-butylphenyl)-N,N′-bis (phenyl) benzidine)
SLG-Single layer graphene
PEG-polyethylene glycol
PA-n-propylamine
P3HT-Poly(3-hexylthiophene-2,5-diyl)
GO QDs-Graphene oxide quantum dots
NPs-Nanoparticles
MB-Methylene blue
Rb-riboflavin
CMG-Chemically modified graphene
QDs- quantum dots
FTO-fluorene doped tin oxide
PPV-poly(*p* -phenylenevinylene)
CNT-Carbon nanotube
SWNT-Single walled carbon nanotube
PANI-Polyaniline
Other symbols/abbreviations
NIR-Near-infrared
HJs-Heterojunctions
FB-forward bias
ESIPT-Intra-molecular proton transfer
QY-Quantum yield
RT-room temperature
E_v, VB-Valance band

E_c,CB-Conduction band
VBM-Valance band maximum
λ_{em}-Emission wavelength
η-efficiency
J_{sc}- short-circuit current density
J_0-saturation current
V_{oc} - open-circuit voltage
FF-Fill factor
χ-The electron affinity
PCE-Power conversion efficiency
DFT-Density functional theory
V_O-oxygen vacancy
Zn_is-zinc interstitial
IOT-indirect optical transitions
PR-Photoresponse
MO-Molecular orbital
PDOS-Partial density of state
EL-Electroluminescence
FET-field-effect transistors
E_F –Fermi level
CBM-Conduction band minimum
LUMO-Lowest unoccupied molecular orbital
HOMO-Highest occupied molecular orbital
Instrumentation
CLSM-confocal laser scanning microscopic
TEM-transmission electron microscopy
DLS-dynamic light scattering
EELS-Electron energy loss spectroscopy
AFM-Atomic force microscopy
CV-Cyclic voltammetry
PLE-photoluminescence excitation
PDS-Photothermal deflection spectroscopy

Acknowledgements

S. V. thanks The Scientific & Technological Research Council of Turkey (TUBITAK) (TUBITAK-BIDEB 2221 – Fellowships for Visiting Scientists and Scientists on Sabbatical) for fellowship. T. U. thanks EU FP7-Marie Curie-IRG NANOWEB (PIRG06-GA-2009-256428) and The Turkish Academy of Sciences–Outstanding Young Scientists Award Program (TUBA-GEBIP) for partial funding.

Notes and references

[a] *UNAM-National Nanotechnology Research Center, Bilkent University, Ankara, 06800 Turkey Fax: +90 (312) 266 4365; Tel: +90 (312) 290 3571; E-mail: svempati01@qub.ac.uk*
[b] *Institute of Materials Science & Nanotechnology, Bilkent University, Ankara, 06800 Turkey Fax: +90 (312) 266 4365; Tel: +90 (312) 290 3571; E-mail: uyar@unam.bilkent.edu.tr*

1 X. Huang, Z. Y. Yin, S. X. Wu, X. Y. Qi, Q. Y. He, Q. C. Zhang, Q. Y. Yan, F. Boey and H. Zhang, *Small*, 2011, **7**, 1876-1902.
2 C. Chung, Y. K. Kim, D. Shin, S. R. Ryoo, B. H. Hong and D. H. Min, *Accounts of Chemical Research*, 2013, **46**, 2211-2224.
3 Y. Chen, J. Wang and Z. M. Liu, *Chinese Journal of Analytical Chemistry*, 2012, **40**, 1772-1779.
4 M. W. Cole, V. H. Crespi, M. S. Dresselhaus, G. Dresselhaus, J. E. Fischer, H. R. Gutierrez, K. Kojima, G. D. Mahan, A. M. Rao, J. O. Sofo, M. Tachibana, K. Wako and Q. H. Xiong, *Journal of Physics-Condensed Matter*, 2010, **22**, 334201.
5 G. Eda and M. Chhowalla, *Advanced Materials*, 2010, **22**, 2392-2415.
6 K. P. Loh, Q. L. Bao, G. Eda and M. Chhowalla, *Nature Chemistry*, 2010, **2**, 1015-1024.
7 Y. Z. Zhou, J. Yang, X. N. Cheng, N. Zhao, H. B. Sun and D. Li, *Rsc Advances*, 2013, **3**, 3391-3398.
8 D. T. Phan, R. K. Gupta, G. S. Chung, A. A. Al-Ghamdi, O. A. Al-Hartomy, F. El-Tantawy and F. Yakuphanoglu, *Solar Energy*, 2012, **86**, 2961-2966.
9 B. Yin, Q. Liu, L. Yang, X. Wu, Z. Liu, Y. Hua, S. Yin and Y. Che, *J. Nanosci. Nanotechnol.*, 2010, **10**, 1934.
10 B. C. Brodie, *Ann. Chim. Phys.*, 1860, **59**, 466-472.
11 L. Staudenmaier, *Ber. Dtsch. Chem. Ges.*, 1898, **31**, 1481–1499.
12 W. Hummers and R. Offeman, *J. Am. Chem. Soc.*, 1958, **80**, 1339.
13 Z. Y. Yin, S. Y. Sun, T. Salim, S. X. Wu, X. A. Huang, Q. Y. He, Y. M. Lam and H. Zhang, *Acs Nano*, 2010, **4**, 5263-5268.
14 B. H. Wee and J. D. Hong, *Advanced Functional Materials*, 2013, **23**, 4657-4666.
15 K. S. Subrahmanyam, P. Kumar, A. Nag and C. N. R. Rao, *Solid State Communications*, 2010, **150**, 1774-1777.
16 S. Vempati, A. Shetty, P. Dawson, K. K. Nand and S.B.Krupanidhi, *J. Cryst. Growth*, 2012, **343**, 7-12.
17 S. Vempati, J. Mitra and P. Dawson, *Nanoscale Res. Lett.*, 2012, **7**, 470.
18 S. Vempati, S. Chirakkara, J. Mitra, P. Dawson, K. K. Nanda and S. B. Krupanidhi, *Appl. Phys. Lett.*, 2012, **100**, 162104.
19 F. Kayaci, S. Vempati, C.O.-Akgun, N. Biyikli and T. Uyar, *Appl. Catal. B.*, 2014, **156-157**, 173-183.
20 F. Kayaci, S. Vempati, C. Ozgit, I. Donmez, N. Biyikli and T. Uyar, *Nanoscale*, 2014, **6**, 5735.
21 S. Vempati, A. Shetty, P. Dawson, K. K. Nanda and S. B. Krupanidhi, *Thin Solid Films*, 2012, **524**, 137-143.
22 F. Kayaci, S. Vempati, I. Donmez, N. Biyikli and T. Uyar, *Nanoscale*, 2014, **DOI: 10.1039/C4NR01887G**.
23 Y. Shen, S. B. Yang, P. Zhou, Q. Q. Sun, P. F. Wang, L. Wan, J. Li, L. Y. Chen, X. B. Wang, S. J. Ding and D. W. Zhang, *Carbon*, 2013, **62**, 157-164.
24 R. Bauld, M. S. Ahmed and G. Fanchini, *Phys. Status Solidi (c)*, 2012, **9**, 2374-2379.
25 X. M. Sun, Z. Liu, K. Welsher, J. T. Robinson, A. Goodwin, S. Zaric and H. J. Dai, *Nano Research*, 2008, **1**, 203-212.
26 Z. Liu, J. T. Robinson, X. Sun and H. Dai, *J. Am. Chem. Soc.* , 2008, **130**, 10876-10877.
27 Y. W. Wang, Y. Y. Fu, Q. L. Peng, S. S. Guo, G. Liu, J. Li, H. H. Yang and G. N. Chen, *Journal of Materials Chemistry B*, 2013, **1**, 5762-5767.
28 F. X. Wang, Z. Y. Gu, W. Lei, W. J. Wang, X. F. Xia and Q. L. Hao, *Sensors and Actuators B-Chemical*, 2014, **190**, 516-522.
29 X. L. Yu, G. J. Zhang, H. B. Cao, X. Q. An, Y. Wang, Z. J. Shu, X. L. An and F. Hua, *New Journal of Chemistry*, 2012, **36**, 2593-2598.
30 E. Morales-Narvaez and A. Merkoci, *Advanced Materials*, 2012, **24**, 3298-3308.

31 M. Nurunnabi, Z. Khatun, K. M. Huh, S. Y. Park, D. Y. Lee, K. J. Cho and Y. K. Lee, *Acs Nano*, 2013, **7**, 6858-6867.

32 X. M. Zhou, G. Liu, J. G. Yu and W. H. Fan, *Journal of Materials Chemistry*, 2012, **22**, 21337-21354.

33 T. D. Nguyen-Phan, E. W. Shin, V. H. Pham, H. Kweon, S. Kim, E. J. Kim and J. S. Chung, *Journal of Materials Chemistry*, 2012, **22**, 20504-20511.

34 S. Essig, C. W. Marquardt, A. Vijayaraghavan, M. Ganzhorn, S. Dehm, F. Hennrich, F. Ou, A. A. Green, C. Sciascia, F. Bonaccorso, K.-P. Bohnen, H. v. Lohneysen, M. M. Kappes, P. M. Ajayan, M. C. Hersam, A. C. Ferrari and R. Krupke, *Nano Letters*, 2010, **10**, 1589-1594.

35 T. V. Cuong, V. H. Pham, Q. T. Tran, S. H. Hahn, J. S. Chung, E. W. Shin and E. J. Kim, *Materials Letters*, 2010, **64**, 399-401.

36 G. Eda, Y. Y. Lin, C. Mattevi, H. Yamaguchi, H. A. Chen, I. S. Chen, C. W. Chen and M. Chhowalla, *Adv. Mater.*, 2010, **22**, 505–509.

37 D. Pan, J. Zhang, Z. Li and M. Wu, *Adv. Mater.*, 2010, **22**, 734.

38 Z. Luo, P. M. Vora, E. J. Mele, A. T. C. Johnson and J. M. Kikkawa, *Appl. Phys. Lett.* , 2009, **94**, 111909.

39 J. L. Chen and X. P. Yan, *J. Mater. Chem.*, 2010, **20**, 4328-4332.

40 V. C. Tung, M. J. Allen, Y. Yang and R. B. Kaner, *Nature Nanotechnology*, 2009, **4**, 25-29.

41 J. Ito, J. Nakamura and A. Natori, *J. Appl. Phys.*, 2008, **103**, 113712.

42 K. A. Mkhoyan, A. W. Contryman, J. Silcox, D. A. Stewart, G. Eda, C. Mattevi, S. Miller and M. Chhowalla, *Nano Letters*, 2009, **9**, 1058-1063.

43 C. Mattevi, G. Eda, S. Agnoli, S. Miller, K. A. Mkhoyan and O. Celik, *Adv. Funct. Mater.*, 2009, **19**, 2577-2583.

44 C. Gomez-Navarro, J. C. Meyer, R. S. Sundaram, A. Chuvilin, S. Kurasch, M. Burghard, K. Kern and U. Kaiser, *Nano Letters*, 2010, **10**, 1144-1148.

45 P. Johari and V. B. Shenoy, *Acs Nano*, 2011, **5**, 7640-7647.

46 I. Jung, D. A. Field, N. J. Clark, Y. Zhu, D. Yang, R. D. Piner, S. Stankovich, D. A. Dikin, H. Geisler, C. A. V. Jr and R. S. Ruoff, *J. Phys. Chem. C*, 2009, **113**, 18480-18486.

47 W. Gao, L. B. Alemany, L. Ci and P. M. Ajayan, *Nat. Chem.*, 2009, **1**, 403.

48 D. Li, M. B. Muller, S. Gilje, R. B. Kaner and G. G. Wallace, *Nat. Nanotechnol.*, 2008, **3**, 101.

49 V. Lee, L. Whittaker, C. Jaye, K. M. Baroudi, D. A. Fischer and S. Banerjee, *Chem. Mater.*, 2009, **21**, 3905.

50 P.-G. Ren, D.-X. Yan, X. Ji, T. Chen and Z.-M. Li, *Nanotechnology*, 2011, **22**, 055705.

51 S. Stankovich, D. A. Dikin, R. D. Piner, K. A. Kohlhaas, A. Kleinhammes, Y. Jia, Y. Wu, S. T. Nguyen and R. S. Ruoff, *Carbon*, 2007, **45**, 1558-1565.

52 S. P. Stankovich, R. D.; Chen, X.; Wu, N.; Nguyen, S. T.; and R. S. Ruoff, *J. Mater. Chem.*, 2006, **16**, 155-158.

53 H. A. Becerril, J. Mao, Z. Liu, R. M. Stoltenberg, Z. Bao and Y. Chen, *Acs Nano*, 2008, **2**, 464-470.

54 H. X. Chang and H. K. Wu, *Advanced Functional Materials*, 2013, **23**, 1984-1997.

55 I. K. Moon, J. Lee, R. S. Ruoff and H. Lee, *Nat. Commun.*, 2010, **1**, 73.

56 A. Bagri, C. Mattevi, M. Acik, Y. J. Chabal, M. Chhowalla and V. B. Shenoy, *Nature Chemistry*, 2010, **2**, 581-587.

57 Y. A. Niu, J. P. Zhao, X. Zhang, X. J. Wang, J. Wu and Y. Li, *Applied Physics Letters*, 2012, **101**, 181903.

58 C. T. Chien, S. S. Li, W. J. Lai, Y. C. Yeh, H. A. Chen, I. S. Chen, L. C. Chen, K. H. Chen, T. Nemoto, S. Isoda, M. Chen, T. Fujita, G. Eda, H. Yamaguchi, M. Chhowalla and C. W. Chen, *Angew. Chem. Int. Ed. Engl.*, 2012, **51**, 6662-6666.

59 A. Mathkar, D. Tozier, P. Cox, P. J. Ong, C. Galande, K. Balakrishnan, A. L. M. Reddy and P. M. Ajayan, *Journal of Physical Chemistry Letters*, 2012, **3**, 986-991.

60 L. B. Tang, X. M. Li, R. B. Ji, K. S. Teng, G. Tai, J. Ye, C. S. Wei and S. P. Lau, *Journal of Materials Chemistry*, 2012, **22**, 5676-5683.

61 N. Li, M. H. Cao and C. W. Hu, *Nanoscale*, 2012, **4**, 6205-6218.

62 S. Bai and X. P. Shen, *Rsc Advances*, 2012, **2**, 64-98.

63 Y. H. Hu, H. Wang and B. Hu, *Chemsuschem*, 2010, **3**, 782-796.

64 X. Yan, B. Li, X. Cui, Q. Wei, K. Tajima and L. Li, *J. Phys. Chem. Lett.*, 2011, **2**, 1119-1124.

65 M. Lotya, Y. Hernandez, P. J. King, R. J. Smith, V. Nicolosi, L. S. Karlsson, F. M. Blighe, S. De, Z. Wang, I. T. McGovern, G. S. Duesberg and J. N. Coleman, *J. Am. Chem. Soc.*, 2009, **131**, 3611–3620.

66 J. T. Yuan, L. P. Ma, S. F. Pei, J. H. Du, Y. Su, W. C. Ren and H. M. Cheng, *Acs Nano*, 2013, **7**, 4233-4241.

67 J. R. Rani, J. Lim, J. Oh, J. W. Kim, H. S. Shin, J. H. Kim, S. Lee and S. C. Jun, *Journal of Physical Chemistry C*, 2012, **116**, 19010-19017.

68 T. Gokus, R. R. Nair, A. Bonetti, M. Bohmler, A. Lombardo, K. S. Novoselov, A. K. Geim, A. C. Ferrari and A. Hartschuh, *Acs Nano*, 2009, **3**, 3963-3968.

69 Z. S. Qian, C. Wang, G. H. Du, J. Zhou, C. C. Chen, J. J. Ma, J. R. Chen and H. Feng, *CrystEngComm*, 2012, **14**, 4976-4979.

70 M. Iliut, A. M. Gabudean, C. Leordean, T. Simon, C. M. Teodorescu and S. Astilean, *Chemical Physics Letters*, 2013, **586**, 127-131.

71 F. DeMichelis, S. Schreiter and A. Tagliaferro, *Phys. Rev. B*, 1995, **51**, 2143-2147.

72 R. R. Robertson and G. A. J. Amaratunga, *J. Appl. Phys.*, 1996, **80**, 2998-3003.

73 M. Koos, M. Veres, M. Fule and I. Pocsik, *Diamond Relat. Mater.*, 2002, **11**, 53-58.

74 Y. Lin, B. Zhou, R. B. Martin, K. B. Henbest, B. A. Harruff, J. E. Riggs, Z.-X. Guo, L. F. Allard and Y.-P. Sun, *J. Phys. Chem. B* 2005, **109**, 14779-14782.

75 Y. P. Sun, B. Zhou, Y. Lin, W. Wang, K. A. S. Fernando, P. Pathak, M. J. Meziani, B. A. Harruff, X. Wang, H. F. Wang, P. G. Luo, H. Yang, M. E. Kose, B. Chen, L. M. Veca and S. Y. Xie, *J. Am. Chem. Soc.*, 2007, **128**, 7756-7757.

76 H. Liu, T. Ye and C. Mao, *Angew. Chem. Int. Ed.*, 2007, **46**, 6473-6475.

77 S. S. Bao, Z. Hua, X. Y. Wang, Y. Zhou, C. F. Zhang, W. G. Tu, Z. G. Zou and M. Xiao, *Optics Express*, 2012, **20**, 28801-28807.

78 F. Yang, M. L. Zhao, B. Z. Zheng, D. Xiao, L. Wu and Y. Guo, *Journal of Materials Chemistry*, 2012, **22**, 25471-25479.

79 M. Melucci, M. Durso, M. Zambianchi, E. Treossi, Z. Y. Xia, I. Manet, G. Giambastiani, L. Ortolani, V. Morandi, F. De Angelis and V. Palermo, *Journal of Materials Chemistry*, 2012, **22**, 18237-18243.

80 W. Lv, C. H. You, S. D. Wu, B. H. Li, Z. P. Zhu, M. Z. Wang, Q. H. Yang and F. Y. Kang, *Carbon*, 2012, **50**, 3233-3239.

81 A. Gupta and S. K. Saha, *Nanoscale*, 2012, **4**, 6562-6567.

82 L. A. Yan, Y. N. Chang, W. Y. Yin, X. D. Liu, D. B. Xiao, G. M. Xing, L. N. Zhao, Z. J. Gu and Y. L. Zhao, *Physical Chemistry Chemical Physics*, 2014, **16**, 1576-1582.

83 R. Thekkayil, H. John and P. Gopinath, *Synthetic Metals*, 2013, **185**, 38-44.

84 M. Wojtoniszak, D. Roginska, B. Machalinski, M. Drozdzik and E. Mijowska, *Materials Research Bulletin*, 2013, **48**, 2636-2639.

85 R. Yamuna, S. Ramakrishnan, K. Dhara, R. Devi, N. K. Kothurkar, E. Kirubha and P. K. Palanisamy, *Journal of Nanoparticle Research*, 2013, **15**, 1399.

86 J. Shang, L. Ma, J. Li, W. Ai, T. Yu and G. G. Gurzadyan, *Sci. Rep.* , 2012, **2**, 792.

87 X.-F. Zhang, X. Shao and S. Liu, *J. Phys. Chem. A*, 2012, **116**, 7308.

88 C. Galande, A. D. Mohite, A. V. Naumov, W. Gao, L. Ci, A. Ajayan, H. Gao, A. Srivastava, R. B. Weisman and P. M. Ajayan, *Sci. Rep.*, 2011, **85**, 1.

89 Q. Mei, K. Zhang, G. Guan, B. Liu, S. Wang and Z. Zhang, *Chem. Commun.*, 2010, **46**, 7319-7321.

90 Z. X. Gan, S. J. Xiong, X. L. Wu, C. Y. He, J. C. Shen and P. K. Chu, *Nano Lett.*, 2011, **11**, 3951-3956.

91 V. Mamidala, L. Polavarapu, J. Balapanuru, K. P. Loh, Q. H. Xu and W. Ji, *Optics Express*, 2010, **18**, 25928-25935.

92 S. Wang, C. T. Nai, X. F. Jiang, Y. H. Pan, C. H. Tan, M. Nesladek, Q. H. Xu and K. P. Loh, *Journal of Physical Chemistry Letters*, 2012, **3**, 2332-2336.

93 L. S. Panchakarla, K. S. Subrahmanyam, S. K. Saha, A. Govindaraj, H. R. Krishnamurthy, U. V. Waghmare and C. N. R. Rao, *Adv. Mater.*, 2009, **21**, 4726-4730.

94 S. R. P. Silva, J. Robertson, Rusli, G. A. J. Amaratunga and J. Schwan, *Philos. Mag. B*, 1996, **74**, 369-386.

95 J. Zhou, C. Booker, R. Li, X. Zhou, T.-K. Sham, X. Sun and Z. Ding, *J. Am. Chem.Soc.*, 2007, **129**, 744-745.

96 Y. Luo, X. Xia, Y. Liang, Y. Zhang, Q. Ren, J. Lia, Z. Jia and Y. Tang, *J. Sol. Stat. Chem.*, 2007, **180**, 1928-1933.

97 Y. Kanemitsu, S. Okamoto, M. Otobe and S. Oda, *Phys. Rev. B*, 1997, **55**, R7375–R7378.

98 G. Eda, C. Mattevi, H. Yamaguchi, H. Kim and M. Chhowalla, *J. Phys. Chem. C*, 2009, **113**, 15768-15771.

99 T. V. Khai, H. G. Na, D. S. Kwak, Y. J. Kwon, H. Ham, K. B. Shim and H. W. Kim, *Journal of Materials Chemistry*, 2012, **22**, 17992-18003.

100 S. Standkovich, R. D. Pinter, X. Chen, N. Wu, S. B. T. Nguyen and R. S. Ruoff, *J. Mater. Chem.*, 2006, **16**, 155.

101 O. C. Compton, D. A. Dikin, K. W. Putz, L. C. Brinson and S. B. T. Nguyen, *Adv. Mater.*, 2010, **22**, 892.

102 H. K. Jeong, M. H. Jin, K. P. So, S. C. Lim and Y. H. Lee, *Journal of Physics D-Applied Physics*, 2009, **42**, 065418.

103 T. V. Cuong, V. H. Pham, E. W. Shin, J. S. Chung, S. H. Hur, E. J. Kim, Q. T. Tran, H. H. Nguyen and P. A. Kohl, *Appl. Phys. Lett.* , 2011, **99**, 041905.

104 S. H. Elder, F. M. Cot, Y. Su, S. M. Heald, A. M. Tyryshkin, M. K. Bowman, Y. Gao, A. G. Joly, M. L. Balmer, A. C. Kolwaite, K. A. Magrini and D. M. Blake, *J. Am. Chem. Soc.* , 2000, **122**, 5138-5146.

105 V. I. Klimov, S. A. Ivanov, J. Nanda, M. Achermann, I. Bezel, J. A. McGuire and A. Piryatinski, *Nature*, 2007, **447**, 441-446.

106 X. F. Zhang, S. P. Liu and X. N. Shao, *J. Lumin.*, 2013, **136**, 32-37.

107 T. Yeh, F. Chan, C. Hsieh and H. Teng, *J. Phys. Chem. C*, 2011, **115**, 22587-22597.

108 H. K. Jeong, C. Yang, B. S. Kim and K.-J. Kim, *Euro. Phys. Lett.*, 2010, **92**, 37005.

109 R. B. Jose, V.; Yamaoka, Y.; Nagase, T.; Makita, Y.; and Y. B. Shinohara, Y.; Ishikawa, M., *Appl. Phys. A: Mater. Sci. Process.*, 2004, **79**, 1833–1838.

110 Y. Shen, P. Zhou, Q. Q. Sun, L. Wan, J. Li, L. Y. Chen, D. W. Zhang and X. B. Wang, *Appl. Phys. Lett.*, 2011, **99**, 141911.

111 S. N. Wang, R. Wang, X. F. Liu, X. W. Wang, D. D. Zhang, Y. J. Guo and X. H. Qiu, *Journal of Physical Chemistry C*, 2012, **116**, 10702-10707.

112 J. Peng, W. Gao, B. K. Gupta, Z. Liu, R. Romero-Aburto, L. H. Ge, L. Song, L. B. Alemany, X. B. Zhan, G. H. Gao, S. A. Vithayathil, B. A. Kaipparettu, A. A. Marti, T. Hayashi, J. J. Zhu and P. M. Ajayan, *Nano Letters*, 2012, **12**, 844-849.

113 X. M. Sun, D. C. Luo, J. F. Liu and D. G. Evans, *Acs Nano*, 2010, **4**, 3381-3389.

114 F. Tuinstra and J. L. Koenig, *J. Chem. Phys.*, 1970, **53**, 1126.

115 D. S. Knight and W. B. White, *J. Mater. Res.*, 1989, **4**, 385-393.

116 Z. J. Zhang, S. Fan, J. L. Huang and C. M. Lieber, *J. Electron. Mater.*, 1996, **25**, 57-61.

117 H. Wehrheit, T. Au, R. Schmechel, S. O. Shalamberidze, G. I. Kalandadze and A. M. Eristavi, *J. Solid State Chem.*, 1999, **154**, 79-86.

118 K. Shirai, S. Emura, S. Gonda and Y. Kumashiro, *J. Appl. Phys.*, 1995, **78**, 3392-3398.

119 S. J. Henley, J. D. Carey and S. R. P. Silva, *Appl. Phys. Lett.* , 2004, **85**, 6236.

120 F. C. Tai, C. Wei, S. H. Chang and W. S. Chen, *J. Raman Spectrosc.*, 2010, **41**, 933-937.

121 K. Erickson, R. Erni, Z. Lee, N. Alem, W. Gannett and A. Zettl, *Adv. Mater.*, 2010, **22**, 4467-4472.

122 D. V. C. Melnikov, J. R., *Phys. Rev. Lett.* , 2004, **92**, 046802.

123 D. Bourissou, O. Guerret, F. P. Gabbai and G. Bertrand, *Chem. Rev.*, 2000, **100**, 39–91.

124 R. Hoffmann, *J. Am. Chem. Soc.*, 1968, **90**, 1475–1476.

125 J. R. Rani, J. Lim, J. Oh, D. Kim, D. Lee, J. W. Kim, H. S. Shin, J. H. Kim and S. C. Jun, *Rsc Advances*, 2013, **3**, 5926-5936.

126 R. Ishikawa, M. Bando, Y. Morimoto and A. Sandhu, *Nanoscale Research Letters*, 2011, **6**, 111.

127 R. Ishikawa, P. J. Ko, M. Bando, Y. Kurokawa, A. Sandhu and M. Konagai, *Nanoscale Research Letters*, 2013, **8**, 534.

128 T. V. Khai, H. G. Na, D. S. Kwak, Y. J. Kwon, H. Ham, K. B. Shim and H. W. Kim, *Chemical Engineering Journal*, 2012, **211**, 369-377.

129 L. B. Tang, R. B. Ji, X. M. Li, K. S. Teng and S. P. Lau, *Journal of Materials Chemistry C*, 2013, **1**, 4908-4915.

130 F. Karlicky, K. K. R. Datta, M. Otyepka and R. Zboril, *Acs Nano*, 2013, **7**, 6434-6464.

131 T. W. Lin, C. Y. Su, X. Q. Zhang, W. J. Zhang, Y. H. Lee, C. W. Chu, H. Y. Lin, M. T. Chang, F. R. Chen and L. J. Li, *Small*, 2012, **8**, 1384-1391.

132 R. Schmechel, H. Werheit, T. U. Kampen and W. Mönch, *J. Sol. Stat. Chem.*, 2004, **177** 566-568.

133 H. Werheit, H. W. Rotter, S. Shalamberidze, A.L.-Jasper and T. Tanaka, *Phys. Stat. Sol. (b)* 2011, **248**, 1275-1279.

134 Y. Z. Lu, Y. Y. Jiang, W. T. Wei, H. B. Wu, M. M. Liu, L. Niu and W. Chen, *Journal of Materials Chemistry*, 2012, **22**, 2929-2934.

135 Z.-B. Liu, Y.-F. Xu, X.-Y. Zhang, X.-L. Zhang, Y.-S. Chen and J.-G. Tian, *J. Phys. Chem. B.*, 2009, **113**, 9681–9686.

136 Y. F. Xu, Z. B. Liu, X. L. Zhang, Y. Wang, J. G. Tian, Y. Huang, Y. F. Ma, X. Y. Zhang and Y. S. Chen, *Advanced Materials*, 2009, **21**, 1275.

137 Y. S. Liu, J. Y. Zhou, X. L. Zhang, Z. B. Liu, X. J. Wan, J. G. Tian, T. Wang and Y. S. Chen, *Carbon*, 2009, **47**, 3113-3121.

138 J. H. Jung, D. S. Cheon, F. Liu, K. B. Lee and T. S. Seo, *Angew. Chem., Int. Ed.*, 2010, **49**, 5708.

139 S. K. Singh, M. K. Singh, M. K. Nayak, S. Kumari, J. J. A. Gracio and D. Dash, *Carbon*, 2011, **49**, 684-692.

140 F. Liu, J. Y. Choi and T. S. Seo, *Biosens. Bioelectron.*, 2010, **25**, 2361.

141 S. H. Alarcon, D. Pagani, J. Bacigalupo and A. C. Olivieri, *J. Mol. Struct.*, 1999, **475**, 233.

142 Z. B. Liu, Y. Wang, X. L. Zhang, Y. F. Xu, Y. S. Chen and J. G. Tian, *Appl. Phys. Lett.*, 2009, **94**, 021902.

143 J. J. Wang, M. Feng and H. B. Zhan, *Optics and Laser Technology*, 2014, **57**, 84-89.

144 X. Q. Zheng, M. Feng and H. B. Zhan, *Journal of Materials Chemistry C*, 2013, **1**, 6759-6766.

145 X. L. Zhang, Z. B. Liu, X. C. Li, Q. Ma, X. D. Chen, J. G. Tian, Y. F. Xu and Y. S. Chen, *Optics Express*, 2013, **21**, 7511-7520.

146 S. Kumar, M. Anija, N. Kamaraju, K. S. Vasu, K. S. Subrahmanyam, A.K. Sood and C. N. R. Rao, *Appl. Phys. Lett.*, 2009, **95**, 191911.

147 P. Chantharasupawong, R. Philip, N. T. Narayanan, P. M. Sudeep, A. Mathkar, P. M. Ajayan and J. Thomas, *Journal of Physical Chemistry C*, 2012, **116**, 25955-25961.

148 B. L. Allen, P. D. Kichambare, P.Gou, I. I. Vlasova, A.A.Kapralov, N. Konduru, V. E. Kagan and A. Star, *Nano Lett.*, 2008, **8**, 3899.

149 J. L. Chen and X. P. Yan, *Chem. Commun.*, 2011, **47**, 3135.

150 L. Minati, G. Speranza, I. Bernagozzi, S. Torrengo, L. Toniutti, B. Rossi, M. Ferrari and A. Chiasera, *J. Phys. Chem. C*, 2010, **114**, 11068.

151 J. Lu, J. Yang, J. Wang, A. Lim, S. Wang and K. P. Loh, *Acs Nano*, 2009, **3**, 2367-2375.

152 S. Kochmann, T. Hirsch and O. S. Wolfbeis, *J. Fluoresc.*, 2012, **22**, 849.

153 W. Zhao, C. Song and P. E. Pehrsson, *J. Am. Chem. Soc.*, 2002, **124**, 12418.

154 Y. Chen and Z. Rosenzweig, *Anal. Chem.*, 2002, **74**, 5132-5138.

155 L.-J. Fan, Y. Zhang, C. B. Murphy, S. E. Angell, M. F. L. Parker, B. R. Flynn and W. E. J. Jr, *Coord. Chem. Rev*, 2009, **253**, 410-422.

156 C. H. Fan, S. Wang, J. W. Hong, G. C. Bazan, K. W. Plaxco and A. J. Heeger, *Proc. Natl. Acad. Sci. U.S.A.*, 2003, **100**, 6297-6301.

157 W. W. Tu, J. P. Lei, S. Y. Zhang and H. X. Ju, *Chemistry-a European Journal*, 2010, **16**, 10771-10777.

158 B. K. Gupta, P. Thanikaivelan, T. N. Narayanan, L. Song, W. Gao, T. Hayashi, A. L. M. Reddy, A. Saha, V. Shanker, M. Endo, A. A. Marti and P. M. Ajayan, *Nano Letters*, 2011, **11**, 5227-5233.

159 G. G. Blasse, B. C., *Luminescent Materials*, Springer, New York, 1994.

160 L. F. d. O. Gomes, K. T.; Neri, C. R.; de Sousa Filho, P. C.; Dal Bianco, M. J.; Ramos, A. P.; Zaniquelli, M. E. D.; Serra, O. A., *J. Lumin.*, 2008, **128**, 1339-1347.

161 R. D. F. Ionescu, T., *J. Lumin.*, 2004, **106**, 133-139.

162 Z. L. Mo, Y. X. Zhao, R. B. Guo, P. W. Liu and T. T. Xie, *Materials and Manufacturing Processes*, 2012, **27**, 494-498.

163 Z. L. Yang, X. J. Shi, J. J. Yuan, H. T. Pu and Y. S. Liu, *Applied Surface Science*, 2010, **257**, 138-142.

164 J. Zou, L. Liu, H. Chen, S. I. Khondaker, R. D. McCullough, Q. Huo and L. Zhai, *Adv. Mater.*, 2008, **20**, 2055-2060.

165 Y. Liang, D. Wu, X. Feng and K. Mullen, *Adv. Mater.*, 2009, **21**, 1-5.

166 Q. Su, S. Pang, V. Alijani, C. Li, X. Feng and K. Mullen, *Adv. Mater.*, 2009, **21**, 3191-3195.

167 S. D. Stranks, C. Weisspfennig, P. Parkinson, M. B. Johnston, L. M. Herz and R. J. Nicholas, *Nano Lett.*, 2011, **11**, 66.

168 Y. M. Tachibana, J.E.; Grätzel, M.; Klug, D.R.; Durrant, J.R., *J. Phys. Chem.*, 1996, **100**, 20056.

169 D. L. Meng, J. H. Sun, S. D. Jiang, Y. Zeng, Y. Li, S. K. Yan, J. X. Geng and Y. Huang, *Journal of Materials Chemistry*, 2012, **22**, 21583-21591.

170 S. Goswami, U. N. Maiti, S. Maiti, S. Nandy, M. K. Mitra and K. K. Chattopadhyay, *Carbon*, 2011, **49**, 2245-2252.

171 Z. G. Tang, Q. M. Liu, I. Khatri, R. Ishikawa, K. Ueno and H. Shirai, in *Phys. Status Solidi (c)*, eds. S. Pizzini, G. Kissinger, H. YamadaKaneta and J. Kang, Wiley-V C H Verlag Gmbh, Weinheim, 2012, vol. 9, pp. 2075-2078.

172 J. J. Fan, S. W. Liu and J. G. Yu, *Journal of Materials Chemistry*, 2012, **22**, 17027-17036.

173 J. M. Kroon, N. J. Bakker, H. J. P. Smit, P. Liska, K. R. Thampi, P. Wang, S. M. Zakeeruddin, M. Gratzel, A. Hinsch, S. Hore, U. Wurfel, R. Sastrawan, J. R. Durrant, E. Palomares, H. Pettersson, T. Gruszecki, J. Walter, K. Skupien and G. E. Tulloch, *Progr. Photovolt.: Res. Appl.*, 2007, **15**, 1-18.

174 H. F. Liang, W. Ren, J. H. Su and C. L. Cai, *Thin Solid Films*, 2012, **521**, 163-167.

175 G. D. Sharma, M. L. Keshtov, A. R. Khokhlov, D. Tasis and C. Galiotis, *Organic Electronics*, 2014, **15**, 348-355.

176 H. X. Chang, Z. H. Sun, M. Saito, Q. H. Yuan, H. Zhang, J. H. Li, Z. C. Wang, T. Fujita, F. Ding, Z. J. Zheng, F. Yan, H. K. Wu, M. W. Chen and Y. Ikuhara, *Acs Nano*, 2013, **7**, 6310-6320.

177 Y. Lin, K. Zhang, W. F. Chen, Y. D. Liu, Z. G. Geng, J. Zeng, N. Pan, L. F. Yan, X. P. Wang and J. G. Hou, *Acs Nano*, 2010, **4**, 3033-3038.

178 S. M. Z. Islam, T. Gayen, M. Seredych, T. J. Bandosz and R. Alfano, *Optical Components and Materials X*, 2013, **8621**, 86211T-86211.

179 F. Zou, Y. A. Yu, N. Cao, L. Z. Wu and J. F. Zhi, *Scripta Materialia*, 2011, **64**, 621-624.

180 H. Q. Sun, S. Z. Liu, S. M. Liu and S. B. Wang, *Applied Catalysis B-Environmental*, 2014, **146**, 162-168.

181 N. Farhangi, R. R. Chowdhury, Y. Medina-Gonzalez, M. B. Ray and P. A. Charpentier, *Applied Catalysis B-Environmental*, 2011, **110**, 25-32.

182 V. Stengl, J. Henych, P. Vomacka and M. Slusna, *Photochemistry and Photobiology*, 2013, **89**, 1038-1046.

183 G. Singh, A. Choudhary, D. Haranath, A. G. Joshi, N. Singh, S. Singh and R. Pasricha, *Carbon*, 2011, **50**, 385-394.

184 S. Ameen, M. S. Akhtar, H. K. Seo and H. S. Shin, *Materials Letters*, 2013, **100**, 261-265.

185 H. R. Pant, B. Pant, H. J. Kim, A. Amarjargal, C. H. Park, L. D. Tijing, E. K. Kim and C. S. Kim, *Ceramics International*, 2013, **39**, 5083-5091.

186 M. Ahmad, E. Ahmed, Z. L. Hong, N. R. Khalid, W. Ahmed and A. Elhissi, *Journal of Alloys and Compounds*, 2013, **577**, 717-727.

187 M. Y. Wang, J. R. Huang, Z. W. Tong, W. H. Li and J. Chen, *Journal of Alloys and Compounds*, 2013, **568**, 26-35.

188 P. Wang, T. Jiang, C. Zhu, Y. Zhai, D. Wang and S. Dong, *Nano Res.*, 2010, **3**, 794.

189 S. Kaveri, L. Thirugnanam, M. Dutta, J. Ramasamy and N. Fukata, *Ceramics International*, 2013, **39**, 9207-9214.

190 R. C. Pawar and C. S. Lee, *Materials Chemistry and Physics*, 2013, **141**, 686-693.

191 H. T. Hu, X. B. Wang, F. M. Liu, J. C. Wang and C. H. Xu, *Synthetic Metals*, 2011, **161**, 404-410.

192 A. F. Zedan, S. Sappal, S. Moussa and M. S. El-Shall, *Journal of Physical Chemistry C*, 2010, **114**, 19920-19927.

193 J. Chu, X. Li and P. Xu, *Journal of Materials Chemistry*, 2011, **21**, 11283-11287.

194 G. Y. Chen, D. J. Wang, C. Liang, Z. Y. Wei, W. X. Zhang, J. C. Liang and D. M. Wang, *Rare Metal Materials and Engineering*, 2012, **41**, 1153-1155.

195 H. G. Wei, J. H. Zhu, S. J. Wu, S. Y. Wei and Z. H. Guo, *Polymer*, 2013, **54**, 1820-1831.

196 D. I. Son, B. W. Kwon, D. H. Park, W. S. Seo, Y. Yi, B. Angadi, C. L. Lee and W. K. Choi, *Nature Nanotechnology*, 2012, **7**, 465-471.

197 H. D. Zeng, Y. Cao, S. F. Xie, J. H. Yang, Z. H. Tang, X. Y. Wang and L. Y. Sun, *Nanoscale Research Letters*, 2013, **8**, 133.

198 S. Vempati, Y. Ertas and T. Uyar, *J. Phys. Chem. C*, 2013, **17**, 21609–21618.

199 J. J. Ding, M. Q. Wang, J. P. Deng, W. Y. Gao, Z. Yang, C. X. Ran and X. Y. Zhang, *Journal of Alloys and Compounds*, 2014, **582**, 29-32.

200 G. Williams and P. V. Kamat, *Langmuir*, 2009, **25**, 13869-13873.

201 B. Wei, M. Hsu, P. Su, H. Lin, R. Wu and H. A. Lai, *Sensor. Actuat. B Chem.*, 2004, **101**, 81-89.

202 L. L. Zhang, R. Zhou and X. S. Zhao, *J. Mater Chem*, 2010, **20**, 5983-5992.

203 N. Zhang, Y. H. Zhang, X. Y. Pan, X. Z. Fu, S. Q. Liu and Y. J. Xu, *Journal of Physical Chemistry C*, 2011, **115**, 23501-23511.

204 C. Nethravathi, T.Nisha, N.Ravishankar, C.Shivakumara and M. Rajamathi, *Carbon*, 2009, **47**, 2054-2059.

205 B. T. Raut, M. A. Chougule, S. Sen, R. C. Pawar, C. S. Lee and V. B. Patil, *Ceram. Int.*, 2012, **38**, 3999-4007.

206 A. Cao, Z. Liu, S. Chu, M. Wu, Z. Ye, Z. Cai, Y. Chang, S. Wang, Q. Gong and Y. Liu, *Adv. Mater.*, 2010, **22**, 103.

207 Z. Lu, C. X. Guo, H. B. Yang, Y. Qiao, J. Guo and C. M. Li, *J. Colloid Interface Sci.*, 2011, **353**, 588.

208 H. Dong, W. Gao, F. Yan, H. Ji and H. Ju, *Anal. Chem.*, 2010, **82**, 5511.

209 T. Sasaki and M. Watanabe, *J. Phys. Chem. B*, 1997, **101**, 10159-10161.

210 N. D. Abazovic, M. I. Comor, M. D. Dramicanin, D.J. Jovanovic, S. P. Ahrenkiel and J. M. Nedeljkovic, *J. Phys. Chem. B.*, 2006, **110**, 25366-25370.

211 Y. T. Liang, B. K. Vijayan, K. A. Gray and M. C. Hersam, *Nano Lett.*, 2011, **11**, 2865-2870.

212 W. Tu, Y. Zhou, Q. Liu, Z. Tian, J. Gao, X. Chen, H. Zhang, J. Liu and Z. Zou, *Adv. Funct. Mater.*, 2012, **22**, 1215–1221.

213 L. Y. Cheng, J. Zhou, Q. Zou, Y. T. Long and H. Tian, *Rsc Advances*, 2012, **2**, 4623-4626.

214 N.Karousis, A. S. D. Sandanayaka, T. Hasobe, S. P. Economopoulos, E. Sarantopoulou and N. Tagmatarchis, *J. Mater. Chem.*, 2011, **21**, 109.

215 R. Stalder, C. Grand, J. Subbiah, F. So and J. R. Reynolds, *Polym. Chem.*, 2012, **3**, 89.